

A First Search for coincident Gravitational Waves and High Energy Neutrinos using LIGO, VIRGO and ANTARES data from 2007

The ANTARES Collaboration, the LIGO Scientific Collaboration and the VIRGO Collaboration

The ANTARES Collaboration:

S. Adrián-Martínez¹, I. Al Samarai², A. Albert³, M. André⁴, M. Anghinolfi⁵, G. Anton⁶, S. Anvar⁷, M. Ardid¹, T. Astraatmadja^{8,39}, J.-J. Aubert², B. Baret⁹, S. Basa¹⁰, V. Bertin², S. Biagi^{11,12}, C. Bigongiari¹³, C. Bogazzi⁸, M. Bou-Cabo¹, B. Bouhou⁹, M.C. Bouwhuis⁸, J. Brunner², J. Bustó², A. Capone^{14,15}, C. Cárloganu¹⁶, J. Carr², S. Cecchini¹¹, Z. Charif², Ph. Charvis¹⁷, T. Chiarusi¹¹, M. Circella¹⁸, R. Coniglione¹⁹, L. Core², H. Costantini², P. Coyle², A. Creusot⁹, C. Curtil², G. De Bonis^{14,15}, M.P. Decowski⁸, I. Dekeyser²⁰, A. Deschamps¹⁷, C. Distefano¹⁹, C. Donzaud^{9,21}, D. Dornic^{13,2}, Q. Dorosti²², D. Drouhin³, T. Eberl⁶, U. Emanuele¹³, A. Enzenhöfer⁶, J.-P. Ernenwein², S. Escoffier², K. Fehn⁶, P. Fermani^{14,15}, M. Ferri¹, S. Ferry²³, V. Flaminio^{24,25}, F. Folger⁶, U. Fritsch⁶, J.-L. Fuda²⁰, S. Galatà², P. Gay¹⁶, K. Geyer⁶, G. Giacomelli^{11,12}, V. Giordano¹⁹, J.P. Gómez-González¹³, K. Graf⁶, G. Guillard¹⁶, G. Hallewell², M. Hamal²⁶, H. van Haren²⁷, A.J. Heijboer⁸, Y. Hello¹⁷, J.J. Hernández-Rey¹³, B. Herold⁶, J. Hößl⁶, C.C. Hsu⁸, M. de Jong^{8,39}, M. Kadler²⁸, O. Kalekin⁶, A. Kappes^{6,40}, U. Katz⁶, O. Kavatsyuk²², P. Kooijman^{8,29,30}, C. Kopper^{8,6}, A. Kouchner⁹, I. Kreykenbohm²⁸, V. Kulikovskiy^{31,5}, R. Lahmann⁶, G. Lambard¹³, G. Larosa¹, D. Lattuada¹⁹, D. Lefèvre²⁰, G. Lim^{8,30}, D. Lo Presti^{32,33}, H. Loehner²², S. Loucatos²³, F. Louis⁷, S. Mangano¹³, M. Marcelin¹⁰, A. Margiotta^{11,12}, J.A. Martínez-Mora¹, A. Meli⁶, T. Montaruli^{18,34}, M. Morganti^{24,41}, L. Moscico^{9,23,†}, H. Motz⁶, M. Neff⁶, E. Nezri¹⁰, D. Palioselitis⁸, G.E. Pāvāļas³⁵, K. Payet²³, J. Petrovic⁸, P. Piattelli¹⁹, V. Popa³⁵, T. Pradier³⁶, E. Presani⁸, C. Racca³, C. Reed⁸, G. Riccobene¹⁹, C. Richardt⁶, R. Richter⁶, C. Rivière², A. Robert²⁰, K. Roensch⁶, A. Rostovtsev³⁷, J. Ruiz-Rivas¹³, M. Rujoiu³⁵, G.V. Russo^{32,33}, D.F.E. Samtleben⁸, A. Sánchez-Losa¹³, P. Sapienza¹⁹, J. Schmid⁶, J. Schnabel⁶, F. Schöck⁶, J.-P. Schuller²³, F. Schüssler²³, T. Seitz⁶, R. Shanidze⁶, F. Simeone^{14,15}, A. Spies⁶, M. Spurio^{11,12}, J.J.M. Steijger⁸, Th. Stolarczyk²³, M. Taiuti^{5,38}, C. Tamburini²⁰, A. Trovato³², B. Vallage²³, C. Vallée², V. Van Elewyck⁹, M. Vecchi², P. Vernin²³, E. Visser⁸, S. Wagner⁶, G. Wijnker⁸, J. Wilms²⁸, E. de Wolf^{8,30}, H. Yepes¹³, D. Zaborov³⁷, J.D. Zornoza¹³, J. Zúñiga¹³

The LIGO Scientific Collaboration and the VIRGO Collaboration:

J. Aasi⁴², J. Abadie⁴², B. P. Abbott⁴², R. Abbott⁴², T. D. Abbott⁴³, M. Abernathy⁴⁴, T. Accadia⁴⁵, F. Acernese^{46,48}, C. Adams⁴⁹, T. Adams⁵⁰, P. Addresso⁴⁸, R. Adhikari⁴², C. Affeldt^{52,53}, M. Agathos⁸, K. Agatsuma⁵⁵, P. Ajith⁴², B. Allen^{52,56,53}, A. Allocca^{24,57}, E. Amador Ceron⁵⁶, D. Amariutei⁵⁸, S. B. Anderson⁴², W. G. Anderson⁵⁶, K. Arai⁴², M. C. Araya⁴², S. Ast^{52,53}, S. M. Aston⁴⁹, P. Astone¹⁴, D. Atkinson⁵⁹, P. Aufmuth^{53,52}, C. Aulbert^{52,53}, B. E. Aylott⁶⁰, S. Babak⁶¹, P. Baker⁶², G. Ballardín⁶³, S. Ballmer⁶⁴, Y. Bao⁵⁸, J. C. B. Barayoga⁴², D. Barker⁵⁹, F. Barone^{46,48}, B. Barr⁴⁴, L. Barsotti⁶⁵, M. Barsuglia⁹,

M. A. Barton⁵⁹, I. Bartos⁶⁶, R. Bassiri^{44,67}, M. Bastarrika⁴⁴, A. Basti^{24,25}, J. Batch⁵⁹, J. Bauchrowitz^{52,53}, Th. S. Bauer⁸, M. Bebronne⁴⁵, D. Beck⁶⁷, B. Behnke⁶¹, M. Bejger⁷⁰, M.G. Beker⁸, A. S. Bell⁴⁴, C. Bell⁴⁴, I. Belopolski⁶⁶, M. Benacquista⁷⁴, J. M. Berliner⁵⁹, A. Bertolini^{52,53}, J. Betzwieser⁴⁹, N. Beveridge⁴⁴, P. T. Beyersdorf⁷⁵, T. Bhadbade⁶⁷, I. A. Bilenko⁷⁶, G. Billingsley⁴², J. Birch⁴⁹, R. Biswas⁷⁴, M. Bitossi²⁴, M. A. Bizouard⁷⁷, E. Black⁴², J. K. Blackburn⁴², L. Blackburn⁷⁹, D. Blair⁸⁰, B. Bland⁵⁹, M. Blom⁸, O. Bock^{52,53}, T. P. Bodiya⁶⁵, C. Bogan^{52,53}, C. Bond⁶⁰, R. Bondarescu⁸¹, F. Bondu⁸³, L. Bonelli^{24,25}, R. Bonnand⁸⁴, R. Bork⁴², M. Born^{52,53}, V. Boschi²⁴, S. Bose⁸⁵, L. Bosi⁸⁶, S. Braccini^{24,†}, C. Bradaschia²⁴, P. R. Brady⁵⁶, V. B. Braginsky⁷⁶, M. Branchesi^{88,89}, J. E. Brau⁹⁰, J. Breyer^{52,53}, T. Briant⁹¹, D. O. Bridges⁴⁹, A. Brillet⁸², M. Brinkmann^{52,53}, V. Brisson⁷⁷, M. Britzger^{52,53}, A. F. Brooks⁴², D. A. Brown⁶⁴, T. Bulik⁶⁹, H. J. Bulten^{8,54}, A. Buonanno⁹², J. Burguet–Castell⁹³, D. Buskulic⁴⁵, C. Buy⁹, R. L. Byer⁶⁷, L. Cadonati⁹⁴, G. Cagnoli^{74,84}, E. Calloni^{46,47}, J. B. Camp⁷⁹, P. Campsie⁴⁴, K. Cannon⁹⁵, B. Canuel⁶³, J. Cao⁹⁶, C. D. Capano⁹², F. Carbognani⁶³, L. Carbone⁶⁰, S. Caride⁹⁷, S. Caudill⁹⁸, M. Cavaglia⁹⁹, F. Cavalier⁷⁷, R. Cavalieri⁶³, G. Cella²⁴, C. Cepeda⁴², E. Cesarini⁸⁹, T. Chalermongsak⁴², P. Charlton¹⁰⁰, E. Chassande-Mottin⁹, W. Chen⁹⁶, X. Chen⁸⁰, Y. Chen¹⁰¹, A. Chincarini⁵, A. Chiummo⁶³, H. S. Cho¹⁰², J. Chow¹⁰³, N. Christensen¹⁰⁴, S. S. Y. Chua¹⁰³, C. T. Y. Chung¹⁰⁵, S. Chung⁸⁰, G. Ciani⁵⁸, F. Clara⁵⁹, D. E. Clark⁶⁷, J. A. Clark⁹⁴, J. H. Clayton⁵⁶, F. Cleva⁸², E. Coccia^{106,107}, P.-F. Cohadon⁹¹, C. N. Colacino^{24,25}, A. Colla^{14,15}, M. Colombini¹⁵, A. Conte^{14,15}, R. Conte⁴⁸, D. Cook⁵⁹, T. R. Corbitt⁶⁵, M. Cordier⁷⁵, N. Cornish⁶², A. Corsi⁴², C. A. Costa^{98,109}, M. Coughlin¹⁰⁴, J.-P. Coulon⁸², P. Couvares⁶⁴, D. M. Coward⁸⁰, M. Cowart⁴⁹, D. C. Coyne⁴², J. D. E. Creighton⁵⁶, T. D. Creighton⁷⁴, A. M. Cruise⁶⁰, A. Cumming⁴⁴, L. Cunningham⁴⁴, E. Cuoco⁶³, R. M. Cutler⁶⁰, K. Dahl^{52,53}, M. Damjanic^{52,53}, S. L. Danilishin⁸⁰, S. D’Antonio¹⁰⁶, K. Danzmann^{52,53}, V. Dattilo⁶³, B. Daudert⁴², H. Daveloza⁷⁴, M. Davier⁷⁷, E. J. Daw¹¹⁰, R. Day⁶³, T. Dayanga⁸⁵, R. De Rosa^{46,47}, D. DeBra⁶⁷, G. Debreczeni¹¹¹, J. Degallaix⁸⁴, W. Del Pozzo⁸, T. Dent⁵⁰, V. Dergachev⁴², R. DeRosa⁹⁸, S. Dhurandhar¹¹², L. Di Fiore⁴⁶, A. Di Lieto^{24,25}, I. Di Palma^{52,53}, M. Di Paolo Emilio^{106,108}, A. Di Virgilio²⁴, M. Díaz⁷⁴, A. Dietz^{45,99}, F. Donovan⁶⁵, K. L. Dooley^{52,53}, S. Doravari⁴², S. Dorsher¹¹³, M. Drago^{114,115}, R. W. P. Drever¹¹⁸, J. C. Driggers⁴², Z. Du⁹⁶, J.-C. Dumas⁸⁰, S. Dwyer⁶⁵, T. Eberle^{52,53}, M. Edgar⁴⁴, M. Edwards⁵⁰, A. Effler⁹⁸, P. Ehrens⁴², G. Endrőczy¹¹¹, R. Engel⁴², T. Etzel⁴², K. Evans⁴⁴, M. Evans⁶⁵, T. Evans⁴⁹, M. Factourovich⁶⁶, V. Fafone^{106,107}, S. Fairhurst⁵⁰, B. F. Farr¹¹⁹, M. Favata⁵⁶, D. Fazi¹¹⁹, H. Fehrmann^{52,53}, D. Feldbaum⁵⁸, I. Ferrante^{24,25}, F. Ferrini⁶³, F. Fidecaro^{24,25}, L. S. Finn⁸¹, I. Fiori⁶³, R. P. Fisher⁶⁴, R. Flaminio⁸⁴, S. Foley⁶⁵, E. Forisi⁴⁹, L. A. Forte⁴⁶, N. Fotopoulos⁴², J.-D. Fournier⁸², J. Franc⁸⁴, S. Franco⁷⁷, S. Frasca^{14,15}, F. Frasconi²⁴, M. Frede^{52,53}, M. A. Frei¹²⁰, Z. Frei¹²¹, A. Freise⁶⁰, R. Frey⁹⁰, T. T. Fricke^{52,53}, D. Friedrich^{52,53}, P. Fritschel⁶⁵, V. V. Frolov⁴⁹, M.-K. Fujimoto⁵⁵, P. J. Fulda⁶⁰, M. Fyffe⁴⁹, J. Gair¹²², M. Galimberti⁸⁴, L. Gammaitoni^{86,87}, J. Garcia⁵⁹, F. Garuffi^{46,47}, M. E. Gáspár¹¹¹, G. Gelencser¹²¹, G. Gemme⁵, E. Genin⁶³, A. Gennai²⁴, L. Á. Gergely¹²³, S. Ghosh⁸⁵, J. A. Giaime^{98,49}, S. Giampanis⁵⁶, K. D. Giardino⁴⁹, A. Giazotto²⁴, S. Gil-Casanova⁹³, C. Gill⁴⁴, J. Gleason⁵⁸, E. Goetz^{52,53}, G. González⁹⁸, M. L. Gorodetsky⁷⁶, S. Goßler^{52,53}, R. Gouaty⁴⁵,

C. Graef^{52,53}, P. B. Graff¹²², M. Granata⁸⁴, A. Grant⁴⁴, C. Gray⁵⁹, R. J. S. Greenhalgh¹²⁴,
A. M. Gretarsson¹²⁵, C. Griffo⁴³, H. Grote^{52,53}, K. Grover⁶⁰, S. Grunewald⁶¹, G. M. Guidi^{88,89},
C. Guido⁴⁹, R. Gupta¹¹², E. K. Gustafson⁴², R. Gustafson⁹⁷, J. M. Hallam⁶⁰, D. Hammer⁵⁶,
G. Hammond⁴⁴, J. Hanks⁵⁹, C. Hanna^{42,126}, J. Hanson⁴⁹, J. Harms¹¹⁸, G. M. Harry¹²⁷,
I. W. Harry⁶⁴, E. D. Harstad⁹⁰, M. T. Hartman⁵⁸, K. Haughian⁴⁴, K. Hayama⁵⁵, J.-F. Hayau⁸³,
J. Heefner⁴²,†, A. Heidmann⁹¹, M. C. Heintze⁴⁹, H. Heitmann⁸², P. Hello⁷⁷, G. Hemming⁶³,
M. A. Hendry⁴⁴, I. S. Heng⁴⁴, A. W. Heptonstall⁴², V. Herrera⁶⁷, M. Heurs^{52,53}, M. Hewitson^{52,53},
S. Hild⁴⁴, D. Hoak⁹⁴, K. A. Hodge⁴², K. Holt⁴⁹, M. Holtrop¹²⁸, T. Hong¹⁰¹, S. Hooper⁸⁰,
J. Hough⁴⁴, E. J. Howell⁸⁰, B. Hughey⁵⁶, S. Husa⁹³, S. H. Huttner⁴⁴, T. Huynh-Dinh⁴⁹,
D. R. Ingram⁵⁹, R. Inta¹⁰³, T. Isogai¹⁰⁴, A. Ivanov⁴², K. Izumi⁵⁵, M. Jacobson⁴², E. James⁴²,
Y. J. Jang¹¹⁹, P. Jaranowski⁷¹, E. Jesse¹²⁵, W. W. Johnson⁹⁸, D. I. Jones¹²⁹, R. Jones⁴⁴,
R.J.G. Jonker⁸, L. Ju⁸⁰, P. Kalmus⁴², V. Kalogera¹¹⁹, S. Kandhasamy¹¹³, G. Kang¹³⁰,
J. B. Kanner^{92,79}, M. Kasprzack^{63,77}, R. Kasturi¹³¹, E. Katsavounidis⁶⁵, W. Katzman⁴⁹,
H. Kaufer^{52,53}, K. Kaufman¹⁰¹, K. Kawabe⁵⁹, S. Kawamura⁵⁵, F. Kawazoe^{52,53}, D. Keitel^{52,53},
D. Kelley⁶⁴, W. Kells⁴², D. G. Keppel⁴², Z. Keresztes¹²³, A. Khalaidovski^{52,53}, F. Y. Khalili⁷⁶,
E. A. Khazanov¹³², B. K. Kim¹³⁰, C. Kim¹³³, H. Kim^{52,53}, K. Kim¹³⁴, N. Kim⁶⁷, Y. M. Kim¹⁰²,
P. J. King⁴², D. L. Kinzel⁴⁹, J. S. Kissel⁶⁵, S. Klimenko⁵⁸, J. Kline⁵⁶, K. Kokeyama⁹⁸,
V. Kondrashov⁴², S. Koranda⁵⁶, W. Z. Korth⁴², I. Kowalska⁶⁹, D. Kozak⁴², V. Kringel^{52,53},
B. Krishnan⁶¹, A. Królak^{68,72}, G. Kuehn^{52,53}, P. Kumar⁶⁴, R. Kumar⁴⁴, R. Kurdyumov⁶⁷,
P. Kwee⁶⁵, P. K. Lam¹⁰³, M. Landry⁵⁹, A. Langley¹¹⁸, B. Lantz⁶⁷, N. Lastzka^{52,53}, C. Lawrie⁴⁴,
A. Lazzarini⁴², A. Le Roux⁴⁹, P. Leaci⁶¹, C. H. Lee¹⁰², H. K. Lee¹³⁴, H. M. Lee¹³⁵,
J. R. Leong^{52,53}, I. Leonor⁹⁰, N. Leroy⁷⁷, N. Letendre⁴⁵, V. Lhuillier⁵⁹, J. Li⁹⁶, T. G. F. Li⁸,
P. E. Lindquist⁴², V. Litvine⁴², Y. Liu⁹⁶, Z. Liu⁵⁸, N. A. Lockerbie¹³⁶, D. Lodhia⁶⁰, J. Logue⁴⁴,
M. Lorenzini⁸⁸, V. Lorette⁷⁸, M. Lormand⁴⁹, G. Losurdo⁸⁸, J. Lough⁶⁴, M. Lubinski⁵⁹,
H. Lück^{52,53}, A. P. Lundgren^{52,53}, J. Macarthur⁴⁴, E. Macdonald⁴⁴, B. Machenschalk^{52,53},
M. MacInnis⁶⁵, D. M. Macleod⁵⁰, M. Mageswaran⁴², K. Mailand⁴², E. Majorana¹⁴,
I. Maksimovic⁷⁸, V. Malvezzi¹⁰⁶, N. Man⁸², I. Mandel⁶⁰, V. Mandic¹¹³, M. Mantovani²⁴,
F. Marchesoni⁸⁶, F. Marion⁴⁵, S. Márka⁶⁶, Z. Márka⁶⁶, A. Markosyan⁶⁷, E. Maros⁴², J. Marque⁶³,
F. Martelli^{88,89}, I. W. Martin⁴⁴, R. M. Martin⁵⁸, J. N. Marx⁴², K. Mason⁶⁵, A. Masserot⁴⁵,
F. Matichard⁶⁵, L. Matone⁶⁶, R. A. Matzner¹³⁷, N. Mavalvala⁶⁵, G. Mazzolo^{52,53}, R. McCarthy⁵⁹,
D. E. McClelland¹⁰³, S. C. McGuire¹³⁸, G. McIntyre⁴², J. McIver⁹⁴, G. D. Meadors⁹⁷,
M. Mehmet^{52,53}, T. Meier^{53,52}, A. Melatos¹⁰⁵, A. C. Melissinos¹³⁹, G. Mendell⁵⁹,
D. F. Menéndez⁸¹, R. A. Mercer⁵⁶, S. Meshkov⁴², C. Messenger⁵⁰, M. S. Meyer⁴⁹, H. Miao¹⁰¹,
C. Michel⁸⁴, L. Milano^{46,47}, J. Miller¹⁰³, Y. Minenkov¹⁰⁶, C. M. F. Mingarelli⁶⁰,
V. P. Mitrofanov⁷⁶, G. Mitselmakher⁵⁸, R. Mittleman⁶⁵, B. Moe⁵⁶, M. Mohan⁶³,
S. R. P. Mohapatra⁹⁴, D. Moraru⁵⁹, G. Moreno⁵⁹, N. Morgado⁸⁴, A. Morgia^{106,107}, T. Mori⁵⁵,
S. R. Morriss⁷⁴, S. Mosca^{46,47}, K. Mossavi^{52,53}, B. Mours⁴⁵, C. M. Mow–Lowry¹⁰³,
C. L. Mueller⁵⁸, G. Mueller⁵⁸, S. Mukherjee⁷⁴, A. Mullavey^{98,103}, H. Müller-Ebhardt^{52,53},
J. Munch¹⁴⁰, D. Murphy⁶⁶, P. G. Murray⁴⁴, A. Mytidis⁵⁸, T. Nash⁴², L. Naticchioni^{14,15},
V. Necula⁵⁸, J. Nelson⁴⁴, I. Neri^{86,87}, G. Newton⁴⁴, T. Nguyen¹⁰³, A. Nishizawa⁵⁵, A. Nitz⁶⁴,

F. Nocera⁶³, D. Nolting⁴⁹, M. E. Normandin⁷⁴, L. Nuttall⁵⁰, E. Ochsner⁵⁶, J. O’Dell¹²⁴,
E. Oelker⁶⁵, G. H. Ogin⁴², J. J. Oh¹⁴¹, S. H. Oh¹⁴¹, R. G. Oldenberg⁵⁶, B. O’Reilly⁴⁹,
R. O’Shaughnessy⁵⁶, C. Osthelder⁴², C. D. Ott¹⁰¹, D. J. Ottaway¹⁴⁰, R. S. Ottens⁵⁸,
H. Overmier⁴⁹, B. J. Owen⁸¹, A. Page⁶⁰, L. Palladino^{106,108}, C. Palomba¹⁴, Y. Pan⁹²,
C. Pankow⁵⁶, F. Paoletti^{24,63}, R. Paoletti^{24,57}, M. A. Papa^{61,56}, M. Parisi^{46,47}, A. Pasqualetti⁶³,
R. Passaquieti^{24,25}, D. Passuello²⁴, M. Pedraza⁴², S. Penn¹³¹, A. Perreca⁶⁴, G. Persichetti^{46,47},
M. Phelps⁴², M. Pichot⁸², M. Pickenpack^{52,53}, F. Piergiovanni^{88,89}, V. Pierro⁵¹, M. Pihlaja¹¹³,
L. Pinard⁸⁴, I. M. Pinto⁵¹, M. Pitkin⁴⁴, H. J. Pletsch^{52,53}, M. V. Plissi⁴⁴, R. Poggiani^{24,25},
J. Pöld^{52,53}, F. Postiglione⁴⁸, C. Poux⁴², M. Prato⁵, V. Predoi⁵⁰, T. Prestegard¹¹³, L. R. Price⁴²,
M. Prijatelj^{52,53}, M. Principe⁵¹, S. Privitera⁴², R. Prix^{52,53}, G. A. Prodi^{114,115}, L. G. Prokhorov⁷⁶,
O. Puncken^{52,53}, M. Punturo⁸⁶, P. Puppo¹⁴, V. Quetschke⁷⁴, R. Quitzow-James⁹⁰, F. J. Raab⁵⁹,
D. S. Rabeling^{8,54}, I. Rácz¹¹¹, H. Radkins⁵⁹, P. Raffal^{66,121}, M. Rakhmanov⁷⁴, C. Ramet⁴⁹,
B. Rankins⁹⁹, P. Rapagnani^{14,15}, V. Raymond¹¹⁹, V. Re^{106,107}, C. M. Reed⁵⁹, T. Reed¹⁴²,
T. Regimbau⁸², S. Reid⁴⁴, D. H. Reitze⁴², F. Ricci^{14,15}, R. Riesen⁴⁹, K. Riles⁹⁷, M. Roberts⁶⁷,
N. A. Robertson^{42,44}, F. Robinet⁷⁷, C. Robinson⁵⁰, E. L. Robinson⁶¹, A. Rocchi¹⁰⁶, S. Roddy⁴⁹,
C. Rodriguez¹¹⁹, M. Rodruck⁵⁹, L. Rolland⁴⁵, J. G. Rollins⁴², J. D. Romano⁷⁴, R. Romano^{46,48},
J. H. Romie⁴⁹, D. Rosińska^{70,73}, C. Röver^{52,53}, S. Rowan⁴⁴, A. Rüdiger^{52,53}, P. Ruggi⁶³,
K. Ryan⁵⁹, F. Salemi^{52,53}, L. Sammut¹⁰⁵, V. Sandberg⁵⁹, S. Sankar⁶⁵, V. Sannibale⁴²,
L. Santamaría⁴², I. Santiago-Prieto⁴⁴, G. Santostasi¹⁴³, E. Saracco⁸⁴, B. Sassolas⁸⁴,
B. S. Sathyaprakash⁵⁰, P. R. Saulson⁶⁴, R. L. Savage⁵⁹, R. Schilling^{52,53}, R. Schnabel^{52,53},
R. M. S. Schofield⁹⁰, B. Schulz^{52,53}, B. F. Schutz^{61,50}, P. Schwinberg⁵⁹, J. Scott⁴⁴, S. M. Scott¹⁰³,
F. Seifert⁴², D. Sellers⁴⁹, D. Sentenac⁶³, A. Sergeev¹³², D. A. Shaddock¹⁰³, M. Shaltev^{52,53},
B. Shapiro⁶⁵, P. Shawhan⁹², D. H. Shoemaker⁶⁵, T. L. Sidery⁶⁰, X. Siemens⁵⁶, D. Sigg⁵⁹,
D. Simakov^{52,53}, A. Singer⁴², L. Singer⁴², A. M. Sintes⁹³, G. R. Skelton⁵⁶, B. J. J. Slagmolen¹⁰³,
J. Slutsky⁹⁸, J. R. Smith⁴³, M. R. Smith⁴², R. J. E. Smith⁶⁰, N. D. Smith-Lefebvre⁶⁵,
K. Somiya¹⁰¹, B. Sorazu⁴⁴, F. C. Speirits⁴⁴, L. Sperandio^{106,107}, M. Stefszky¹⁰³, E. Steinert⁵⁹,
J. Steinlechner^{52,53}, S. Steinlechner^{52,53}, S. Steplewski⁸⁵, A. Stochino⁴², R. Stone⁷⁴, K. A. Strain⁴⁴,
S. E. Strigin⁷⁶, A. S. Stroer⁷⁴, R. Sturani^{88,89}, A. L. Stuver⁴⁹, T. Z. Summerscales¹⁴⁴, M. Sung⁹⁸,
S. Susmithan⁸⁰, P. J. Sutton⁵⁰, B. Swinkels⁶³, G. Szeifert¹²¹, M. Tacca⁶³, L. Taffarelo¹¹⁶,
D. Talukder⁸⁵, D. B. Tanner⁵⁸, S. P. Tarabrin^{52,53}, R. Taylor⁴², A. P. M. ter Braack⁸,
P. Thomas⁵⁹, K. A. Thorne⁴⁹, K. S. Thorne¹⁰¹, E. Thrane¹¹³, A. Thüring^{53,52}, C. Titsler⁸¹,
K. V. Tokmakov¹³⁶, C. Tomlinson¹¹⁰, A. Toncelli^{24,25}, M. Tonelli^{24,25}, O. Torre^{24,57},
C. V. Torres⁷⁴, C. I. Torrie^{42,44}, E. Tournefier⁴⁵, F. Travasso^{86,87}, G. Traylor⁴⁹, M. Tse⁶⁶,
D. Ugolini¹⁴⁵, H. Vahlbruch^{53,52}, G. Vajente^{24,25}, J. F. J. van den Brand^{8,54}, C. Van Den Broeck⁸,
S. van der Putten⁸, A. A. van Veggel⁴⁴, S. Vass⁴², M. Vasuth¹¹¹, R. Vaulin⁶⁵, M. Vavoulidis⁷⁷,
A. Vecchio⁶⁰, G. Vedovato¹¹⁶, J. Veitch⁵⁰, P. J. Veitch¹⁴⁰, K. Venkateswara¹⁴⁶, D. Verkindt⁴⁵,
F. Vetrano^{88,89}, A. Viceré^{88,89}, A. E. Villar⁴², J.-Y. Vinet⁸², S. Vitale⁸, H. Vocca⁸⁶, C. Vorvick⁵⁹,
S. P. Vyatchanin⁷⁶, A. Wade¹⁰³, L. Wade⁵⁶, M. Wade⁵⁶, S. J. Waldman⁶⁵, L. Wallace⁴²,
Y. Wan⁹⁶, M. Wang⁶⁰, X. Wang⁹⁶, A. Wanner^{52,53}, R. L. Ward⁹, M. Was⁷⁷, M. Weinert^{52,53},
A. J. Weinstein⁴², R. Weiss⁶⁵, T. Welborn⁴⁹, L. Wen^{101,80}, P. Wessels^{52,53}, M. West⁶⁴,

T. Westphal^{52,53}, K. Wette^{52,53}, J. T. Whelan¹²⁰, S. E. Whitcomb^{42,80}, D. J. White¹¹⁰,
B. F. Whiting⁵⁸, K. Wiesner^{52,53}, C. Wilkinson⁵⁹, P. A. Willems⁴², L. Williams⁵⁸, R. Williams⁴²,
B. Willke^{52,53}, M. Wimmer^{52,53}, L. Winkelmann^{52,53}, W. Winkler^{52,53}, C. C. Wipf⁶⁵,
A. G. Wiseman⁵⁶, H. Wittel^{52,53}, G. Woan⁴⁴, R. Wooley⁴⁹, J. Worden⁵⁹, J. Yablon¹¹⁹,
I. Yakushin⁴⁹, H. Yamamoto⁴², K. Yamamoto^{115,117}, C. C. Yancey⁹², H. Yang¹⁰¹,
D. Yeaton-Massey⁴², S. Yoshida¹⁴⁷, M. Yvert⁴⁵, A. Zadrożny⁷², M. Zanolin¹²⁵, J.-P. Zendri¹¹⁶,
F. Zhang⁹⁶, L. Zhang⁴², C. Zhao⁸⁰, N. Zotov^{142,†}, M. E. Zucker⁶⁵, J. Zweizig⁴²

¹Institut d'Investigació per a la Gestió Integrada de les Zones Costaneres (IGIC) - Universitat Politècnica de València. C/ Paranimf 1 , 46730 Gandia, Spain.

²CPPM, Aix-Marseille Université, CNRS/IN2P3, Marseille, France

³GRPHE - Institut universitaire de technologie de Colmar, 34 rue du Grillenbreit BP 50568 - 68008 Colmar, France

⁴Technical University of Catalonia, Laboratory of Applied Bioacoustics, Rambla Exposició, 08800 Vilanova i la Geltrú, Barcelona, Spain

⁵INFN - Sezione di Genova, Via Dodecaneso 33, 16146 Genova, Italy

⁶Friedrich-Alexander-Universität Erlangen-Nürnberg, Erlangen Centre for Astroparticle Physics, Erwin-Rommel-Str. 1, 91058 Erlangen, Germany

⁷Direction des Sciences de la Matière - Institut de recherche sur les lois fondamentales de l'Univers - Service d'Electronique des Détecteurs et d'Informatique, CEA Saclay, 91191 Gif-sur-Yvette Cedex, France

⁸Nikhef, Science Park, Amsterdam, The Netherlands

⁹APC - Laboratoire AstroParticule et Cosmologie, UMR 7164 (CNRS, Université Paris 7 Diderot, CEA, Observatoire de Paris) 10, rue Alice Domon et Léonie Duquet 75205 Paris Cedex 13, France

¹⁰LAM - Laboratoire d'Astrophysique de Marseille, Pôle de l'Étoile Site de Château-Gombert, rue Frédéric Joliot-Curie 38, 13388 Marseille Cedex 13, France

¹¹INFN - Sezione di Bologna, Viale C. Berti-Pichat 6/2, 40127 Bologna, Italy

¹²Dipartimento di Fisica dell'Università, Viale Berti Pichat 6/2, 40127 Bologna, Italy

¹³IFIC - Instituto de Física Corpuscular, Edificios Investigación de Paterna, CSIC - Universitat de València, Apdo. de Correos 22085, 46071 Valencia, Spain

¹⁴INFN -Sezione di Roma, P.le Aldo Moro 2, 00185 Roma, Italy

¹⁵Dipartimento di Fisica dell'Università La Sapienza, P.le Aldo Moro 2, 00185 Roma, Italy

¹⁶Clermont Université, Université Blaise Pascal, CNRS/IN2P3, Laboratoire de Physique Corpusculaire, BP 10448, 63000 Clermont-Ferrand, France

¹⁷Géoazur - Université de Nice Sophia-Antipolis, CNRS/INSU, IRD, Observatoire de la Côte d'Azur and Université Pierre et Marie Curie, BP 48, 06235 Villefranche-sur-mer, France

¹⁸INFN - Sezione di Bari, Via E. Orabona 4, 70126 Bari, Italy

¹⁹INFN - Laboratori Nazionali del Sud (LNS), Via S. Sofia 62, 95123 Catania, Italy

²⁰COM - Centre d'Océanologie de Marseille, CNRS/INSU et Université de la Méditerranée, 163 Avenue de Luminy, Case 901, 13288 Marseille Cedex 9, France

²¹Univ Paris-Sud , 91405 Orsay Cedex, France

²²Kernfysisch Versneller Instituut (KVI), University of Groningen, Zernikelaan 25, 9747 AA Groningen, The Netherlands

²³Direction des Sciences de la Matière - Institut de recherche sur les lois fondamentales de l'Univers - Service de Physique des Particules, CEA Saclay, 91191 Gif-sur-Yvette Cedex, France

²⁴INFN - Sezione di Pisa, Largo B. Pontecorvo 3, 56127 Pisa, Italy

-
- ²⁵Dipartimento di Fisica dell'Università, Largo B. Pontecorvo 3, 56127 Pisa, Italy
- ²⁶University Mohammed I, Laboratory of Physics of Matter and Radiations, B.P.717, Oujda 6000, Morocco
- ²⁷Royal Netherlands Institute for Sea Research (NIOZ), Landsdiep 4,1797 SZ 't Horntje (Texel), The Netherlands
- ²⁸Dr. Remeis-Sternwarte and ECAP, Universität Erlangen-Nürnberg, Sternwartstr. 7, 96049 Bamberg, Germany
- ²⁹Universiteit Utrecht, Faculteit Betawetenschappen, Princetonplein 5, 3584 CC Utrecht, The Netherlands
- ³⁰Universiteit van Amsterdam, Instituut voor Hoge-Energie Fysica, Science Park 105, 1098 XG Amsterdam, The Netherlands
- ³¹Moscow State University,Skobeltsyn Institute of Nuclear Physics,Leninskie gory, 119991 Moscow, Russia
- ³²INFN - Sezione di Catania, Viale Andrea Doria 6, 95125 Catania, Italy
- ³³Dipartimento di Fisica ed Astronomia dell'Università, Viale Andrea Doria 6, 95125 Catania, Italy
- ³⁴Département de Physique Nucléaire et Corpusculaire, Université de Genève, 1211, Geneva, Switzerland
- ³⁵Institute for Space Sciences, R-77125 Bucharest, Măgurele, Romania
- ³⁶IPHC-Institut Pluridisciplinaire Hubert Curien - Université de Strasbourg et CNRS/IN2P3 23 rue du Loess, BP 28, 67037 Strasbourg Cedex 2, France
- ³⁷ITEP - Institute for Theoretical and Experimental Physics, B. Chermushkinskaya 25, 117218 Moscow, Russia
- ³⁸Dipartimento di Fisica dell'Università, Via Dodecaneso 33, 16146 Genova, Italy
- ³⁹ Also at University of Leiden, the Netherlands
- ⁴⁰ On leave of absence at the Humboldt-Universität zu Berlin
- ⁴¹ Also at Accademia Navale di Livorno, Livorno, Italy
- ⁴²LIGO - California Institute of Technology, Pasadena, CA 91125, USA
- ⁴³California State University Fullerton, Fullerton CA 92831 USA
- ⁴⁴SUPA, University of Glasgow, Glasgow, G12 8QQ, United Kingdom
- ⁴⁵Laboratoire d'Annecy-le-Vieux de Physique des Particules (LAPP), Université de Savoie, CNRS/IN2P3, F-74941 Annecy-Le-Vieux, France
- ⁴⁶INFN, Sezione di Napoli, Complesso Universitario di Monte S.Angelo, I-80126 Napoli, Italy
- ⁴⁷Università di Napoli 'Federico II', Complesso Universitario di Monte S.Angelo, I-80126 Napoli, Italy
- ⁴⁸Università di Salerno, I-84084 Fisciano (Salerno), Italy
- ⁴⁹LIGO - Livingston Observatory, Livingston, LA 70754, USA
- ⁵⁰Cardiff University, Cardiff, CF24 3AA, United Kingdom
- ⁵¹University of Sannio at Benevento, I-82100 Benevento, Italy and INFN (Sezione di Napoli), Italy
- ⁵²Albert-Einstein-Institut, Max-Planck-Institut für Gravitationsphysik, D-30167 Hannover, Germany
- ⁵³Leibniz Universität Hannover, D-30167 Hannover, Germany
- ⁵⁴VU University Amsterdam, De Boelelaan 1081, 1081 HV Amsterdam, the Netherlands
- ⁵⁵National Astronomical Observatory of Japan, Tokyo 181-8588, Japan

-
- ⁵⁶University of Wisconsin–Milwaukee, Milwaukee, WI 53201, USA
- ⁵⁷Università di Siena, I-53100 Siena, Italy
- ⁵⁸University of Florida, Gainesville, FL 32611, USA
- ⁵⁹LIGO - Hanford Observatory, Richland, WA 99352, USA
- ⁶⁰University of Birmingham, Birmingham, B15 2TT, United Kingdom
- ⁶¹Albert-Einstein-Institut, Max-Planck-Institut für Gravitationsphysik, D-14476 Golm, Germany
- ⁶²Montana State University, Bozeman, MT 59717, USA
- ⁶³European Gravitational Observatory (EGO), I-56021 Cascina (PI), Italy
- ⁶⁴Syracuse University, Syracuse, NY 13244, USA
- ⁶⁵LIGO - Massachusetts Institute of Technology, Cambridge, MA 02139, USA
- ⁶⁶Columbia University, New York, NY 10027, USA
- ⁶⁷Stanford University, Stanford, CA 94305, USA
- ⁶⁸IM-PAN 00-956 Warsaw, Poland
- ⁶⁹Astronomical Observatory Warsaw University 00-478 Warsaw, Poland
- ⁷⁰CAMK-PAN 00-716 Warsaw, Poland
- ⁷¹Białystok University 15-424 Białystok, Poland
- ⁷²NCBJ 05-400 Świerk-Otwock, Poland
- ⁷³Institute of Astronomy 65-265 Zielona Góra, Poland
- ⁷⁴The University of Texas at Brownsville, Brownsville, TX 78520, USA
- ⁷⁵San Jose State University, San Jose, CA 95192, USA
- ⁷⁶Moscow State University, Moscow, 119992, Russia
- ⁷⁷LAL, Université Paris-Sud, IN2P3/CNRS, F-91898 Orsay, France
- ⁷⁸ESPCI, CNRS, F-75005 Paris, France
- ⁷⁹NASA/Goddard Space Flight Center, Greenbelt, MD 20771, USA
- ⁸⁰University of Western Australia, Crawley, WA 6009, Australia
- ⁸¹The Pennsylvania State University, University Park, PA 16802, USA
- ⁸²Université Nice-Sophia-Antipolis, CNRS, Observatoire de la Côte d’Azur, F-06304 Nice, France
- ⁸³Institut de Physique de Rennes, CNRS, Université de Rennes 1, 35042 Rennes, France
- ⁸⁴Laboratoire des Matériaux Avancés (LMA), IN2P3/CNRS, F-69622 Villeurbanne, Lyon, France
- ⁸⁵Washington State University, Pullman, WA 99164, USA
- ⁸⁶INFN, Sezione di Perugia, I-06123 Perugia, Italy
- ⁸⁷Università di Perugia, I-06123 Perugia, Italy
- ⁸⁸INFN, Sezione di Firenze, I-50019 Sesto Fiorentino, Italy

-
- ⁸⁹Università degli Studi di Urbino 'Carlo Bo', I-61029 Urbino, Italy
- ⁹⁰University of Oregon, Eugene, OR 97403, USA
- ⁹¹Laboratoire Kastler Brossel, ENS, CNRS, UPMC, Université Pierre et Marie Curie, 4 Place Jussieu, F-75005 Paris, France
- ⁹²University of Maryland, College Park, MD 20742 USA
- ⁹³Universitat de les Illes Balears, E-07122 Palma de Mallorca, Spain
- ⁹⁴University of Massachusetts - Amherst, Amherst, MA 01003, USA
- ⁹⁵Canadian Institute for Theoretical Astrophysics, University of Toronto, Toronto, Ontario, M5S 3H8, Canada
- ⁹⁶Tsinghua University, Beijing 100084 China
- ⁹⁷University of Michigan, Ann Arbor, MI 48109, USA
- ⁹⁸Louisiana State University, Baton Rouge, LA 70803, USA
- ⁹⁹The University of Mississippi, University, MS 38677, USA
- ¹⁰⁰Charles Sturt University, Wagga Wagga, NSW 2678, Australia
- ¹⁰¹Caltech-CaRT, Pasadena, CA 91125, USA
- ¹⁰²Pusan National University, Busan 609-735, Korea
- ¹⁰³Australian National University, Canberra, ACT 0200, Australia
- ¹⁰⁴Carleton College, Northfield, MN 55057, USA
- ¹⁰⁵The University of Melbourne, Parkville, VIC 3010, Australia
- ¹⁰⁶INFN, Sezione di Roma Tor Vergata, I-00133 Roma, Italy
- ¹⁰⁷Università di Roma Tor Vergata, I-00133 Roma, Italy
- ¹⁰⁸Università dell'Aquila, I-67100 L'Aquila, Italy
- ¹⁰⁹Instituto Nacional de Pesquisas Espaciais, 12227-010 - São José dos Campos, SP, Brazil
- ¹¹⁰The University of Sheffield, Sheffield S10 2TN, United Kingdom
- ¹¹¹Wigner RCP, RMKI, H-1121 Budapest, Konkoly Thege Miklós út 29-33, Hungary
- ¹¹²Inter-University Centre for Astronomy and Astrophysics, Pune - 411007, India
- ¹¹³University of Minnesota, Minneapolis, MN 55455, USA
- ¹¹⁴INFN, Gruppo Collegato di Trento, I-38050 Povo, Trento, Italy
- ¹¹⁵Università di Trento, I-38050 Povo, Trento, Italy
- ¹¹⁶INFN, Sezione di Padova, I-35131 Padova, Italy
- ¹¹⁷Università di Padova, I-35131 Padova, Italy
- ¹¹⁸California Institute of Technology, Pasadena, CA 91125, USA
- ¹¹⁹Northwestern University, Evanston, IL 60208, USA
- ¹²⁰Rochester Institute of Technology, Rochester, NY 14623, USA

ABSTRACT

We present the results of the first search for gravitational wave bursts associated with high energy neutrinos. Together, these messengers could reveal new, hidden sources that are not observed by conventional photon astronomy, particularly at high energy. Our

¹²¹Eötvös Loránd University, Budapest, 1117 Hungary

¹²²University of Cambridge, Cambridge, CB2 1TN, United Kingdom

¹²³University of Szeged, 6720 Szeged, Dóm tér 9, Hungary

¹²⁴Rutherford Appleton Laboratory, HSIC, Chilton, Didcot, Oxon OX11 0QX United Kingdom

¹²⁵Embry-Riddle Aeronautical University, Prescott, AZ 86301 USA

¹²⁶Perimeter Institute for Theoretical Physics, Ontario, N2L 2Y5, Canada

¹²⁷American University, Washington, DC 20016, USA

¹²⁸University of New Hampshire, Durham, NH 03824, USA

¹²⁹University of Southampton, Southampton, SO17 1BJ, United Kingdom

¹³⁰Korea Institute of Science and Technology Information, Daejeon 305-806, Korea

¹³¹Hobart and William Smith Colleges, Geneva, NY 14456, USA

¹³²Institute of Applied Physics, Nizhny Novgorod, 603950, Russia

¹³³Lund Observatory, Box 43, SE-221 00, Lund, Sweden

¹³⁴Hanyang University, Seoul 133-791, Korea

¹³⁵Seoul National University, Seoul 151-742, Korea

¹³⁶University of Strathclyde, Glasgow, G1 1XQ, United Kingdom

¹³⁷The University of Texas at Austin, Austin, TX 78712, USA

¹³⁸Southern University and A&M College, Baton Rouge, LA 70813, USA

¹³⁹University of Rochester, Rochester, NY 14627, USA

¹⁴⁰University of Adelaide, Adelaide, SA 5005, Australia

¹⁴¹National Institute for Mathematical Sciences, Daejeon 305-390, Korea

¹⁴²Louisiana Tech University, Ruston, LA 71272, USA

¹⁴³McNeese State University, Lake Charles, LA 70609 USA

¹⁴⁴Andrews University, Berrien Springs, MI 49104 USA

¹⁴⁵Trinity University, San Antonio, TX 78212, USA

¹⁴⁶University of Washington, Seattle, WA, 98195-4290, USA

¹⁴⁷Southeastern Louisiana University, Hammond, LA 70402, USA

[†]Deceased

search uses neutrinos detected by the underwater neutrino telescope ANTARES in its 5 line configuration during the period January - September 2007, which coincided with the fifth and first science runs of LIGO and VIRGO, respectively. The LIGO-VIRGO data were analysed for candidate gravitational-wave signals coincident in time and direction with the neutrino events. No significant coincident events were observed. We place limits on the density of joint high energy neutrino - gravitational wave emission events in the local universe, and compare them with densities of merger and core-collapse events.

Subject headings: gravitational waves — high energy neutrinos
gravitational waves — high energy neutrinos

1. Introduction

Multi-messenger astronomy is entering a stimulating period with the recent development of experimental techniques that have opened new windows of observation of cosmic radiation in all its components. In particular, both high energy (\gg GeV) neutrinos (HENs) and gravitational waves (GWs), which have not yet been directly observed from astrophysical sources, are new tools for exploring the Universe. While HENs are produced in interactions between accelerated protons and material adjacent to the source, GWs carry information on the dynamics in the central regions of the progenitor.

Several known astrophysical sources are expected to produce both GWs and HENs. Plausible galactic sources of joint emission are Soft Gamma Repeaters (SGRs), X-ray pulsars with soft γ -ray bursting activity which, according to the magnetar model, may be associated with star-quakes (Duncan & Thompson 1992; Thompson & Duncan 1995; van Hoven & Levin 2011). The deformation of the star during the outburst could produce GWs (de Freitas Pacheco 1998; Ioka 2001; Corsi & Owen 2011; Zink et al. 2012), while HENs could potentially emerge from hadron-loaded flares (Aso et al. 2008).

Perhaps the most interesting extragalactic sources are gamma-ray bursts (GRBs) (Kouveliotou et al. 1993). Short-duration bursts ($\lesssim 2$ s) are believed to be produced by the merger of a double neutron star or neutron star - black hole binary (R. Narayan & Piran 1992; Gehrels et al. 2006); such systems will potentially produce short and intense GW emissions with significant associated HEN fluxes (Eichler et al. 1989; Nakar 2007). Long-duration GRBs ($\gtrsim 2$ s) are associated with a particular type of core-collapse supernova (Galama et al. 1998; MacFadyen & Woosley 1999; Hjorth et al. 2003; Stanek et al. 2003; Malesani et al. 2004; Campana et al. 2006; Woosley & Bloom 2006). Several scenarios have been proposed (Davies et al. 2002; Fryer et al. 2002; M. Shibata & Eriguchi 2003; Kotake et al. 2006; Piro & Pfahl 2007; Corsi & Mészáros 2009; Ott 2009; Ott et al. 2011) for GW emission during the gravitational collapse of the rapidly rotating progenitor star and in the pre-GRB phase. In the prompt and afterglow emission phases, HENs with energy

between 10^5 GeV and 10^{10} GeV may be produced by accelerated protons in relativistic shocks and several models predict detectable fluxes in km^3 scale detectors (Bahcall & Waxman 1997; Meszaros 1999; Waxman 2001). Coincident observations of GWs (Kobayashi & Mészáros 2003) and HENs from GRBs could therefore improve our understanding of the details of astrophysical processes connecting the gravitational collapse or merger of compact objects to black-hole formation as well as to the formation of fireballs and relativistic jets.

Particularly intriguing potential sources are choked GRBs, thought to be associated with mildly relativistic, optically thick, baryon-rich jets, leading to only weak or absent gamma-ray emission. Such sources, recently connected to low-luminosity long GRBs (Bromberg et al. 2012), might be promising emitters of GWs and HENs (Meszaros & Waxman 2001).

A more exotic class of sources are cosmic strings, topological defects formed during phase transitions in the early Universe. Emission of gravitational waves is considered the main channel for cosmic string loops to decay. In particular, cosmic string cusps appear to be potential sources of gravitational waves due to the very large Lorentz factor achieved when they contract. Cosmic strings and topological defects in general are also of interest to high energy neutrino astronomy as they can produce particles, including neutrinos, up to the Planck scale (Damour & Vilenkin 2000; Mosquera Cuesta & González 2001; Siemens et al. 2006; Berezhinsky et al. 2011).

In this article we present a new multimessenger analysis, first proposed in Aso et al. (2008); Pradier (2009), and developed, e.g., in Ando et al. (2012): a search for gravitational wave bursts detected by LIGO and VIRGO in temporal and directional coincidence with high energy neutrinos detected by ANTARES. The basic principle is a “triggered” search: HEN candidates are identified in the ANTARES data, then the GW data around the time of the HEN event are analysed for a GW incident from the HEN estimated arrival direction. This method has been applied previously in searches for GWs associated with GRB triggers (Abbott et al. 2010), and has been shown to be more sensitive than a “blind” search of the GW data. The neutrino candidates have been selected using ANTARES data from January to September 2007, when ANTARES was still under construction and operating with only 5 active lines. This period coincides with the fifth LIGO science run (S5) and first VIRGO science run (VSR1), the first joint run of the LIGO-VIRGO network with the detectors operating near their design sensitivities. We analyse a total of 158 HENs detected at times when two or more of the LIGO-VIRGO detectors were operating. ANTARES is sensitive to HENs with energies greater than ~ 100 GeV. The LIGO-VIRGO analysis targets primarily gravitational-wave burst signals with duration $\lesssim 1$ s and frequencies in the 60 Hz - 500 Hz band. The GW search is extended in frequency up to 2000 Hz only for a subset of the HEN events, because the computational cost of such a search with the current GW analysis pipeline is prohibitive, as explained in Section 4.4.

The first requirement imposed for this triggered search for GWs is that the candidate signal be coincident in time, within an astrophysically motivated window, with the neutrino event. Hence by using a subset of the available GW data, the triggered search can be run with a lower detection

threshold than an untriggered search (that scans all available data and looks for simultaneous jumps of energy in all detectors) (Abbott et al. 2010). For example, the false alarm rate for this search is about 100 times lower than in an untriggered search (Abadie et al. 2010), allowing lower thresholds with greater sensitivity to weak GWs.

This paper is organised as follows. In Section 2 we describe the ANTARES, LIGO, and VIRGO detectors and the joint data taking period. Section 3 describes how the HEN sample was selected. Section 4 describes the search for GWs coincident in time and direction with the HEN events. We present the results of the search in Section 5. The statistical analyses of the HEN sample show no sign of associated GWs. We discuss the astrophysical implications of this null result in Section 6 and conclude with considerations of the potential for future joint HEN-GW searches.

2. GW and HEN detectors

2.1. The ANTARES neutrino telescope

Since the Earth acts as a shield against all particles except neutrinos, a neutrino telescope mainly uses the detection of upgoing muons as a signature of muon-neutrino charged-current interactions in the matter around the detector. The ANTARES detector (Astronomy with a Neutrino Telescope and Abyss environmental RESearch) is currently the only deep sea high-energy-neutrino telescope and is operating in the Northern hemisphere (Ageron et al. 2011). The telescope covers an area of about 0.1 km^2 on the sea bed, at a depth of 2475 m, 40 km off the coast of Toulon, France. The detector is a three-dimensional array of photomultiplier tubes (PMTs), hosted in pressure resistant glass spheres, called optical modules (OMs). In its full configuration, it is composed of 12 detection lines, each comprising up to 25 triplets of PMTs, storeys, regularly distributed along 350 m, the first storey being located 100 m above the sea bed. The first detection line was installed and connected in early 2006; the second line was put in operation in September 2006 and three more lines were connected in January 2007, so that a total of 5 lines were taking data in 2007. Five additional lines, together with an instrumentation line (containing an ensemble of oceanographic sensors dedicated to the measurement of environmental parameters), were connected by the end of 2007. The telescope reached its nominal configuration, with 12 lines immersed and taking data, in May 2008.

The three-dimensional grid of PMTs is used to measure the arrival time and position of Cherenkov photons induced by the passage of relativistic charged particles through the sea water. This information, together with the characteristic emission angle of the light (about 43 degrees), is used to determine the direction of the muon and hence infer that of the incident neutrino. The accuracy of the direction information allows to distinguish upgoing muons, produced by neutrinos, from the overwhelming background from downgoing muons, produced by cosmic ray interactions in the atmosphere above the detector. Installing the detector at great depths serves to attenuate this background and also allows to operate the PMTs in a dark environment. At high energies the large

muon range makes the sensitive volume of the detector significantly greater than the instrumented volume. By searching for upgoing muons, the total ANTARES sky coverage is 3.5π sr, with most of the galactic plane being observable and the Galactic Center being visible 70% of the sidereal day.

2.2. Network of interferometers

2.2.1. LIGO

LIGO is a network of interferometric gravitational wave detectors consisting of three interferometers in the USA. These detectors are all kilometer-scale power-recycled Michelson laser interferometers with orthogonal Fabry-Perot arms (Abbott et al. 2009) able to detect the quadrupolar strain in space produced by the GW. Multiple reflections between mirrors located at the end points of each arm extend the effective optical length of each arm, and enhance the sensitivity of the instrument.

There are two LIGO observatories: one located at Hanford, WA and the other at Livingston, LA. The Hanford site houses two interferometers: one with 4 km arms, denoted H1, and a second with 2 km arms, denoted H2. The Livingston observatory has one 4 km interferometer, L1. The observatories are separated by a distance of 3000 km, corresponding to a time-of-flight separation of 10 ms.

The LIGO instruments are designed to detect gravitational waves with frequencies ranging from ~ 40 Hz to several kHz, with a maximum sensitivity near 150 Hz (see Fig 1). In fact, seismic noise dominates at lower frequencies and the sensitivity at intermediate frequencies is determined mainly by thermal noise, with contributions from other sources. Above ~ 200 Hz, laser shot noise corrected for the Fabry-Perot cavity response yields an effective strain noise that rises linearly with frequency.

The average sensitivities of the H1 and L1 detectors during the second year of the S5 run were about 20% better than the first-year averages, while the H2 detector had about the same average sensitivity in both years.

2.2.2. VIRGO

The VIRGO detector, V1, is in Cascina near Pisa, Italy. It is a 3 km long power-recycled Michelson interferometer with orthogonal Fabry Perot arms (Accadia et al. 2012). The main instrumental difference with respect to LIGO is the seismic isolation system based on super-attenuators (Braccini et al. 2005), chains of passive attenuators capable of filtering seismic disturbances. The benefit from super-attenuators is a significant reduction of the detector noise at very low frequency (< 40 Hz) where VIRGO surpasses the LIGO sensitivity. During 2007, above 300 Hz, the VIRGO detector had sensitivity similar to the LIGO 4 km interferometers, while above 500 Hz it is dominated by shot

noise, see Fig 1.

The time-of-flight separation between the VIRGO and Hanford observatories is 27 ms, and 25 ms between VIRGO and Livingston. Due to the different orientation of its arms, the angular sensitivity of VIRGO is complementary to that of the LIGO detectors, VIRGO therefore enhances the sky coverage of the network. Moreover, simultaneous observations of multiple detectors are crucial to reject environmental and instrumental effects.

At the time of writing the LIGO and VIRGO interferometers are undergoing upgrades to “advanced” configurations with distance sensitivity improved by approximately a factor of 10 (Harry et al. 2010). The advanced instruments will commence operations around 2015.

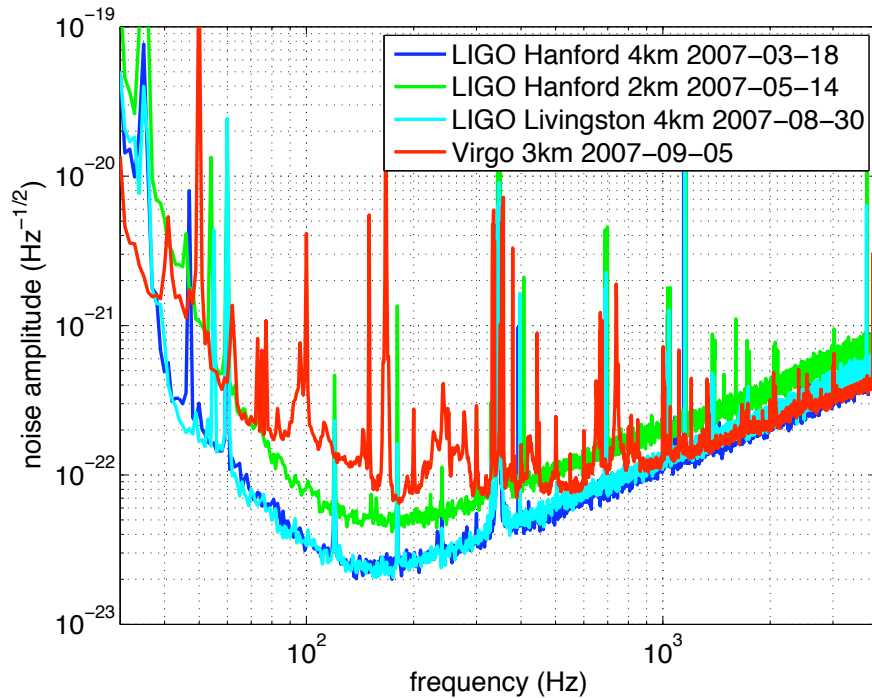


Fig. 1.— Noise amplitude spectral densities of the four LSC and VIRGO detectors during S5

2.3. Joint data taking periods

The fifth LIGO science run, S5 (Abbott et al. 2008a), was held from 2005 November 4 to 2007 October 1. Over one year of science-quality data were collected with all three LIGO interferometers in simultaneous operation at their design sensitivity, with duty factors of 75%, 76%, and 65% for H1, H2, and L1. The VIRGO detector started its first science run, VSR1 (Acernese et al. 2008), on

2007 May 18. The VIRGO duty factor over VSR1 was 78%. During this period, ANTARES was operating in its 5 line configuration. The concomitant set of ANTARES 5-line (5L), VSR1 and S5 data covers the period between January 27 and September 30, 2007; these data are the subject of the analysis presented here.

3. Selection of HEN candidates

3.1. HEN data sample

The ANTARES data sample used in the analysis is composed of runs from 2007 selected according to various quality criteria, based mainly on environmental parameters (e.g. sea current, counting rates), configuration and behaviour of the detector during the given run (e.g. duration of the run, alignment of the detector). Two basic quantities are used to characterise the counting rate of a given OM: the baseline rate (^{40}K activity and bioluminescence) and the burst fraction (flashes of light emitted by marine organisms). The baseline rate represents the most probable counting rate of a given OM computed from the rate distributions in each PMT over the whole run (typically a few hours). The burst fraction corresponds to the fraction of time during which the OM counting rates exceed by more than 20% the estimated baseline. The data selected for this search are required to have a baseline rate below 120 kHz and a burst fraction lower than 40%, with 80% of all OMs being active. With these quality criteria, the active time is 139.7 days out of the 244.8 days of the 5-line period. Finally, when restricting the data to the concomitant period with LIGO/VIRGO, the remaining equivalent time of observation is $T_{\text{obs}} = 104$ days.

3.2. Trigger levels

The ANTARES trigger system is multi-level. The first level is applied *in situ*, while the remaining levels intervene after all data are sent to the shore station and before being written on disk. Trigger decisions are based on calculations done at three levels. The first trigger level, L0, is a simple threshold of about 0.3 photo-electron (pe) equivalent charge applied to the analog signal of the PMT. The second level trigger, L1, is based on two coincident L0 hits in the same storey within 20 ns or hits with large charge (≥ 3 pe or 10 pe depending on the configuration). The L2 trigger requires the presence of at least five L1 hits in a $2.2 \mu\text{s}$ time window (roughly the maximum muon transit time across the detector) and that each pair of L1 hits are causally related according to the following condition: $\Delta t_{ij} \leq d_{ij}n/c + 20$ ns. Here Δt_{ij} and d_{ij} are the time difference and distance between hits i and j , c is the speed of light in vacuum and n is the index of refraction.

3.3. Reconstruction strategy

Hits selected according to the criteria described in Section 3.2 are then combined to reconstruct tracks using their arrival time and charge as measured by the corresponding OM. Muons are assumed to cross the detector at the speed of light along a straight line from which the induced Cherenkov light originates. The time and charge information of the hits in the PMTs is used in a minimisation procedure to obtain the track parameters, namely, its direction (θ, ϕ) and the position (x_0, y_0, z_0) of one track point at a given time t_0 . The reconstruction algorithm used for this analysis is a fast and robust method (Aguilar et al. 2011) which was primarily designed to be used on-line.

3.3.1. Description of the algorithm

The algorithm is based on a χ^2 -minimisation approach. Its strict hit selection leads to a high purity up-down separation while keeping a good efficiency. The exact geometry of the detector is ignored: the detector lines are treated as straight and the 3 OMs of each storey are considered as a single OM centered on the line. Thus, the hit's altitude corresponds to the optical modules altitude. All hits at the same floor in coincidence within 20 ns are merged into one hit. The time of the merged hit is that of the earliest hit in the group and its charge is the sum of the charges. The algorithm uses the L1 hits as a seed for the hit selection. It requests a coincidence of 2 L1 hits in two adjacent floors within 80 ns or 160 ns in two next-to-adjacent floors. The quality of the reconstruction is measured by a χ^2 -like variable with NDF degrees of freedom, based on the time differences between the hit times t_i and the expected arrival time t_i^γ of photons from the track or bright-point (see Section 3.4). The quality function is then extended with a term that accounts for measured hit charges q_i and the calculated photon travel distances d_i^γ :

$$\chi^2 = \frac{1}{NDF} \sum_{i=1}^{N_{\text{hit}}} \left[\frac{\Delta t_i^2}{\sigma_i^2} + \frac{Q(q_i)}{\bar{q}} \frac{D(d_i^\gamma)}{d_0} \right]. \quad (1)$$

In this expression, σ_i is the timing error, set to 10 ns for charges larger than 2.5 pe and to 20 ns otherwise. $\Delta t_i = t_i^\gamma - t_i$ is the time residuals between the hit time t_i and the expected arrival time of the photons t_i^γ from the muon track. In the second term, \bar{q} is the average hit charge calculated from all hits which have been selected for the fit and $d_0 = 50 \text{ m}$ is the typical distance at which the signal in one PMT from a Cherenkov light front is of the order of 1 pe. The function $Q(q_i)$ accounts for the angular acceptance of the OMs, while $D(d_i^\gamma)$ penalises large amplitude hits originating from large distance tracks. A proper cut on the fit quality parameter allows the isolation of a high purity neutrino sample, which is crucial in the subsequent analysis.

3.3.2. Azimuthal degeneracy of the reconstruction

For a particle trajectory reconstructed from a Cherenkov cone giving hits on only two straight detector lines, there always exists an alternative trajectory having an identical χ^2 value, but a different direction. The degenerate trajectory is the mirror image of the original track in the plane formed by the two lines. As a consequence, each event reconstructed with only two lines will have two equiprobable arrival directions, which must be taken into account during the subsequent GW analysis.

3.4. Criteria for HEN event selection

The initial sample of reconstructed events contains both upgoing neutrino induced muons and downgoing muons from cosmic ray interactions in the atmosphere. Some of the atmospheric muons are misreconstructed as upgoing and the selection cuts, based on Monte-Carlo simulations, are devised to reduce this contamination so as to maximise the discovery potential. A minimum of 6 hits on at least 2 lines are required to reconstruct a track. Only upgoing tracks are kept for further analysis. Quality cuts are then applied based on two quantities computed according to equation (1). The first parameter used, χ_t^2 , is the quality factor associated with the reconstructed particle track, whereas the second one, χ_b^2 , is associated with a bright-point, light emitted from a point-like source inside the detector. This rejects events from large electromagnetic showers, likely to appear in downgoing muon bundles for instance.

A cut on χ_b^2 reduces the number of such events and decreases the contribution of misreconstructed muons in the background. Further cuts are applied on χ_t^2 depending on the arrival direction of the candidate - the muon contamination increasing close to the horizon - which reduce the fraction of misreconstructed muons to less than 20% over the whole sample, while optimising the sensitivity (see Section 3.6 and Halladjian (2010)).

Figure 2 shows the distribution of the sine of the declination of the events selected with the final cuts, which is globally consistent with background.

3.5. Angular error

The distribution of the space angle Ω between the true neutrino arrival direction and the reconstructed muon track can be described by a log-normal distribution:

$$P(\Omega) = \frac{1}{\sqrt{2\pi}} \frac{e^{-\frac{1}{2\sigma_0^2} \ln^2 \frac{\Omega - \theta_0}{m_0}}}{(\Omega - \theta_0) \sigma_0}, \quad (2)$$

where θ_0 is a location parameter, σ_0 is related to the shape of the distribution and m_0 is a scaling parameter. This distribution depends on the energy associated to the track (estimated through

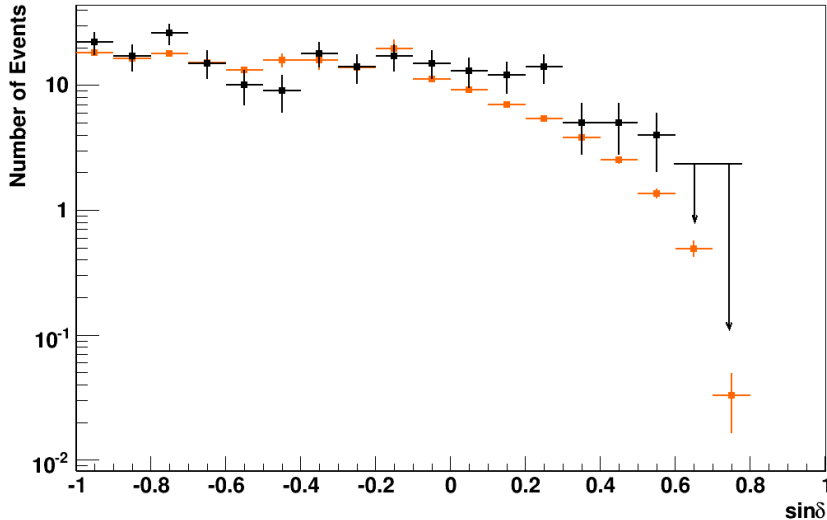


Fig. 2.— Distribution of the sine of the declination δ of selected events (black points), compared to Monte-Carlo expectations (sum of atmospheric muons and atmospheric neutrinos, orange (or grey) points).

the number of photons detected) and its declination. This parametrisation is used during the GW search to compute the significance of a hypothetical signal for the scanned directions inside the angular search window centred around the reconstructed neutrino arrival direction. Figure 3 shows an example of distribution of the space angle for a sample of MC neutrinos with an E^{-2} spectrum, together with the best-fit parametrisation and the 50th and 90th percentiles of the distribution.

One of the main variables to describe the performance of a neutrino telescope is the angular resolution, defined as the median of the distribution of the angle between the true neutrino direction and the reconstructed track, also indicated in Figure 3. This number is estimated from simulations.

For those events of our selected sample reconstructed with at least three lines the angular resolution is, assuming an E^{-2} energy spectrum, $\sim 2.5^\circ$ at 100 GeV, improving to 1° around 100 TeV. For 2-line events, when selecting the reconstructed track closer to the true direction, the angular accuracy varies between 3° at low energy (100 GeV) and 2.5° at high energy (100 TeV).

We define the angular search window for the GW analysis as the 90th percentile of the distribution, also indicated in Figure 3; this window lies between 5° and 10° for 3-line events, depending on declination, and between 10° and 15° for 2-line events.

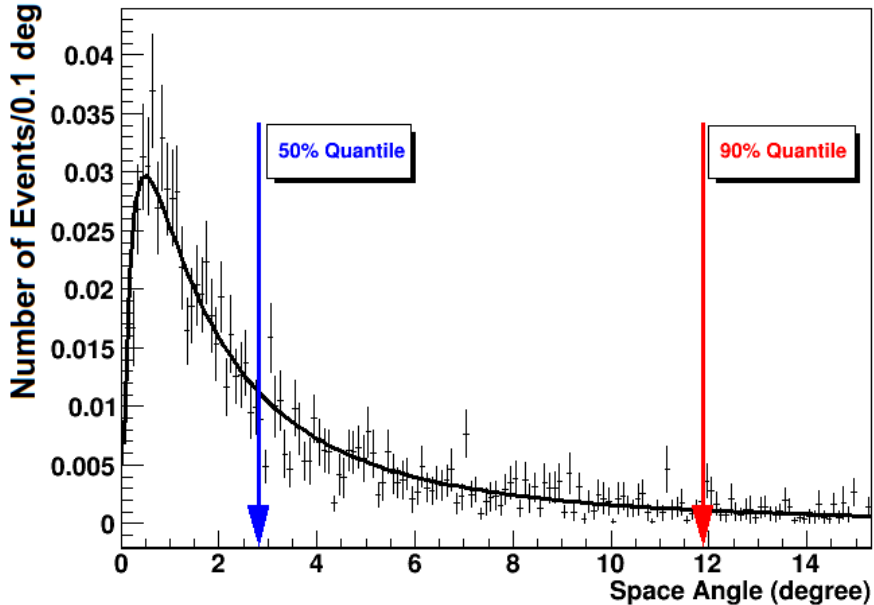


Fig. 3.— Example of space angle distribution with the associated fit to equation (2) obtained with a sample of Monte-Carlo HEN events, for a given declination and a given number of hits. The arrows indicate the 50th (median) and the 90th percentiles of the distribution. The distribution is normalised to unity.

3.6. Analysis sensitivity and selected HEN candidates

The limit-setting potential of the analysis, or sensitivity, has been quantified for the whole 5 line data period. Specifically, the sensitivity is defined as the median 90% upper limit obtained over an ensemble of simulated experiments with no true signal. The sensitivity depends on the declination of the potential source. For our sample and assuming an E^{-2} steady flux, using the selection criteria described, the best sensitivity has been estimated to be $E^2 \frac{dN}{dE} \approx 10^{-6} \text{ GeV cm}^{-2} \text{ s}^{-1}$ and is reached below -47° , the latitude of ANTARES.

With the selection previously described, 181 runs corresponding to 104 days of live time were kept for the analysis. The selection has been divided into events reconstructed with 2 lines and events with at least 3 lines. Each of the mirror solutions for 2 line events will be searched for possible counterparts in the subsequent GW analysis. This results in 216 neutrinos to be analysed: 198 with two possible directions and 18 reconstructed with at least 3 lines. Figure 4 is a sky map of the candidate HEN events, where the degenerate solutions for 2 line events can be seen.

Of these HEN events, 158 occurred at times when at least two gravitational-wave detectors were operating. Since two or more detectors are required to discriminate GW signals from background

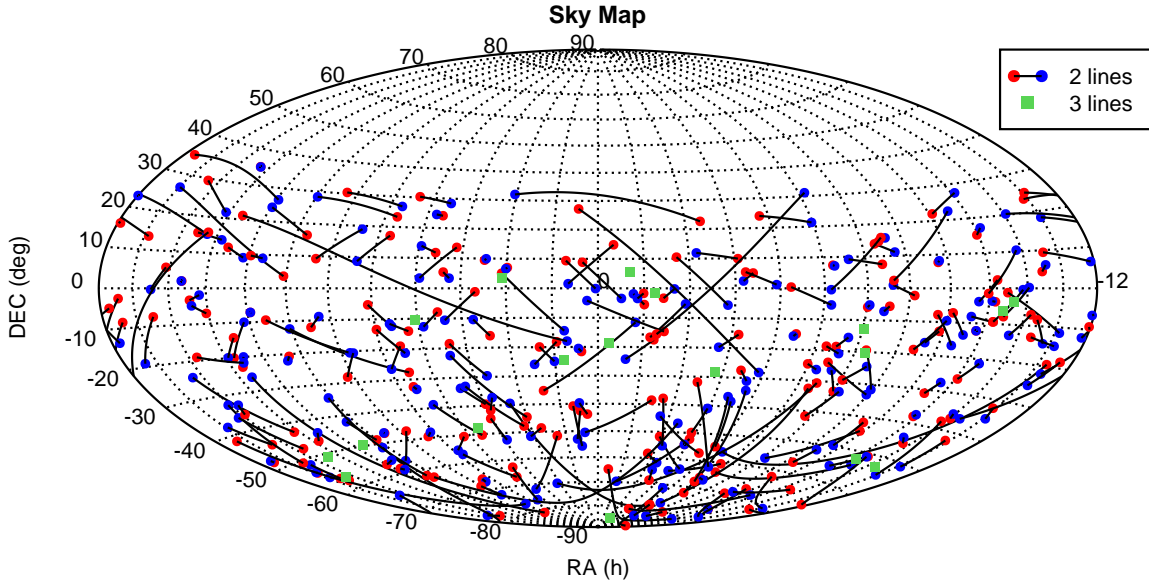


Fig. 4.— Skymap of the selected 216 HEN events in equatorial coordinates. A line connects the associated mirror solutions for events reconstructed with two lines as described in Section 3.3.2.

noise (as described in Section 4.2), in the following we consider only these remaining 158 HEN candidates: 144 2-line events and 14 3-line events¹.

4. GW search method

4.1. Search procedure

One of the simplest searches that may be performed combining GW and HEN data is a triggered analysis that scans GW data around the time of the putative neutrino event by cross-correlating data from pairs of detectors. This search exploits knowledge of the time and direction of the neutrino event to improve the GW search sensitivity. We use the X-PIPELINE algorithm (Sutton et al. 2010), which has been used in similar searches for GWs associated with GRBs (Abbott et al. 2010). X-PIPELINE performs a coherent analysis of data from arbitrary networks of gravitational wave detectors, while being robust against background noise fluctuations. Each trigger is analysed independently of the others, with the analysis parameters optimised based on background noise characteristics and detector performance at the time of that trigger, thereby maximising the search sensitivity.

¹Details of each of these HEN candidate events are given online at the following address : <https://dcc.ligo.org/cgi-bin/DocDB/ShowDocument?docid=p1200006>.

4.2. GW event analysis

In our GW search, a neutrino candidate event is characterised by its arrival time, direction, and angular search window (and mirror-image window, for the 2-line events). Also important is the range of possible time delays (both positive and negative) between the neutrino emission and the associated gravitational-wave emission. This quantity is referred to as the *on-source* window for the neutrino; it is the time interval which is searched for GW signals. We use a symmetric on-source window of ± 496 s (Baret et al. 2011), which is conservative enough to encompass most theoretical models of GW and HEN emission. The maximum expected time delay between GWs and HENs due to a non-zero mass effect for either particle is much smaller than the coincidence windows used.

The basic search procedure follows that used in Abbott et al. (2010). All detectors operating at the time of the trigger and which pass data-quality requirements are used for the GW search. The data from each detector are first whitened and time-delayed according to the sky location being analysed so that a GW signal from that direction would appear simultaneous in each data stream. The data are then Fourier transformed to produce time-frequency maps. The maps are summed coherently (using amplitude and phase) with weighting determined by each detector’s frequency-dependent sensitivity and response to the sky location in question; the weightings are chosen to maximise the signal-to-noise ratio expected for a circularly polarized GW signal, with a marginalisation over possible signal amplitudes. A threshold is placed on the map to retain the largest 1% of pixels by energy (squared amplitude). Surviving pixels are grouped using next-nearest-neighbours clustering; each cluster of pixels is considered as a candidate GW event. The event cluster is assigned a combined energy by summing the energy values of its constituent pixels; this combined energy is used as the ranking statistic for the events.

The circular polarization cut renders the search sensitive to linearly polarized signals too, in fact the performance with these cuts was actually able to detect a 50% of signals at a lower amplitude. Hence the analysis as a detection search was improved by the circular polarization cuts, even in the case of linearly polarized signals. In addition to the marginalised circular polarization sum, other combinations of the data are constructed. Of particular importance are “null” combinations designed to cancel out the GW signal from the given sky location; comparison to corresponding “incoherent” combinations provides powerful tests for identifying events due to background noise fluctuations (“glitches”), as described in (Was et al. 2012). For each combination, the event cluster is assigned a combined energy as the sum of the energy values of its constituent pixels. In addition to these energies, events are characterised by their duration, central time, bandwidth, and central frequency. Also, a second ranking statistic is computed based on a maximum-likelihood analysis of the event assuming power-law distributed background noise with no assumption on the GW polarization; in practice this statistic is often found to provide signal-noise separation due to the non-Gaussian nature of the GW detector noise.

The time-frequency analysis is repeated for Fourier transform lengths of $1/128$, $1/64$, $1/32$,

1/16, 1/8, 1/4 s, to maximise the sensitivity to GW signals of different durations. It is also repeated over a grid of sky positions designed to cover the 90% containment region of the HEN. This grid is designed such that the maximum relative timing error between any pair of GW detectors is less than 0.5 ms. When GW events from different Fourier transforms lengths or sky positions overlap in time-frequency, the highest-ranked event is kept and the others discarded. Finally, the events are decimated to a rate of 0.25 Hz before being written to disk.

This time-frequency analysis is performed for all of the data in the ± 496 s on-source window. To estimate the significance of the resulting GW candidates, the same analysis is repeated for all coincident data in the *off-source* window, defined as all data within ± 1.5 hours of the neutrino time, excluding the on-source interval. The same set of detectors and data-quality requirements as in the on-source analysis are used for the off-source data. These off-source data provide a sample of background that does not contain any signal associated with the neutrino event, but with statistical features similar to the data searched in association with the neutrino. To enlarge the background sample, we also repeat the off-source analysis after applying time shifts of multiples of 6 s to the data from one or more detectors; with such time slides we were able to produce $O(10^3)$ background trials for each HEN.

Finally, the analysis is repeated after “injecting” (adding) simulated GW signals to the on-source data. The amplitudes and morphologies tested are discussed in Section 5.3.1. We use these simulations to optimise and assess the sensitivity of the search, as discussed below.

4.3. GW search optimisation

The sensitivity of searches for gravitational-wave bursts tends to be limited by the presence of non-Gaussian fluctuations of the background noise, known as glitches. To reduce this background, events that overlap in time within known instrumental and/or environmental disturbances are discarded. In addition to this “veto” step, GW consistency tests comparing the coherent and incoherent energies are applied to each event (Was et al. 2012). These tests are applied to the on-source, off-source and injection events; events failing one or more of these tests are discarded. The thresholds are optimised by testing a preset range of thresholds and selecting those which give the best overall detection efficiency at a fixed false alarm probability of 1% when applied to a random sample of background and injection events (the on-source events are *not* used; i.e., this is a blind analysis). These tests also determine which of the two ranking statistics discussed in Section 4.2 (based on circularly polarized GW energy or powerlaw noise) gives the better detection efficiency; the winner is selected as the final ranking statistic.

Once the thresholds have been fixed, these consistency tests are applied to the on-source events and to the remaining off-source and injection events (those not used for tuning). The surviving on-source event with the largest significance (highest energy or powerlaw statistic) is taken to be the best candidate for a gravitational wave signal and is referred to as the loudest event (Brady

et al. 2004). All surviving on-source events are assigned a false alarm probability by comparison to the distribution of loudest events from the off-source trials. Any on-source event with probability $p < 0.01$ is subjected to additional checks to try to determine the origin of the event and additional background time slide trials are performed to improve the accuracy of the false alarm probability estimate.

After the p values have been determined for the loudest events associated with each of the 158 HEN events, the collective set of p values is tested for consistency with the null hypothesis (no GW signal) using the binomial test, discussed in Section 5.2. We also set a frequentist upper limit on the strength of gravitational waves associated with each neutrino trigger, as discussed in Section 5.3.

4.4. Low-frequency and high-frequency GW analyses

Given our knowledge of possible GW sources discussed in Section 1, the most likely detectable signals at extra-galactic distances are in the low-frequency band ($f \lesssim 500$ Hz), where our detectors have maximum sensitivity, see Fig 1. At the same time, the computational cost of the X-PIPELINE analysis increases at high frequencies. This is due in part to the extra data to be analysed, but also to the need for finer-resolution sky grids to keep time delay errors much smaller than one GW period. We therefore split the gravitational wave band into two regions: 60-500 Hz and 500-2000 Hz. The low-frequency band is analysed for all HEN events – such a search is computationally feasible while covering the highest-sensitivity region of the GW detectors. However, compact objects such as neutron stars or collapsar cores have characteristic frequencies for GW emission above 500 Hz. Such emissions might be detectable from galactic sources such as soft gamma repeater giant flares, or possibly from nearby galaxies. Since the computational cost of a high-frequency search for all HEN events is prohibitive with the current analysis pipeline, we perform the 500-2000 Hz analysis on the 3-line HEN events only. The 3-line events are a small subset ($\sim 10\%$) of the total trigger list and have the smallest sky position uncertainties, and therefore the smallest computational cost for processing. To reduce the computational cost further, we use the same sky grid for the high-frequency search as was used at low frequencies, after determining that the loss of sensitivity is acceptable. The high-frequency analysis is performed independently of the low-frequency analysis (independent tuning, background estimation, etc.) using the identical automated procedure. In the following sections we will present the results of the low- frequency and high-frequency searches separately.

5. Coincident search results

5.1. Per-HEN GW candidates

We analysed GW data in coincidence with 158 neutrino candidates for the low frequency search, and 14 neutrino events for the high frequency search. In the low frequency analysis, only one neutrino trigger had a corresponding GW event with false alarm probability below the threshold of $p = 0.01$ to become a candidate event. We found no candidates in the high frequency search. For the low-frequency candidate, additional time shifts totaling 18064 background trials yielded a refined false alarm probability of $p = 0.004$, which is not significant given a trials factor of 158 (this statement is quantified below). This event came from analysis of the H1, H2, and V1 data; follow-up checks were performed, including checks of detector performance at the time as indicated by monitoring programs and operator logs, and scans of data from detector and environmental monitoring equipment to look for anomalous behavior. While these checks did not uncover a physical cause for the event, they did reveal that it occurred during a glitching period in V1. We conclude that we have no clear gravitational wave burst signal associated with any of our sample of 158 neutrino events.

5.2. Search for a cumulative excess: binomial test

A quantitative analysis of the significance of any candidate gravitational-wave event must take account of the trials factor due to the number of neutrino events analysed. We use the binomial test, which has been applied in previous GRB-triggered GW searches ([Abbott et al. 2008b](#), [2010](#)). Under the null hypothesis, the false alarm probabilities p for each HEN loudest event are expected to be uniformly distributed between 0 and 1. The binomial test compares the measured p values to the null distribution to determine if there is a statistically significant excess of (one or more) small p values which may be due to gravitational wave signals.

Briefly, the binomial test sorts the set of N measured loudest event probabilities in ascending order: $p_1 \leq p_2 \leq p_3 \leq \dots \leq p_N$. For each $i \in [1, N_{\text{tail}}]$ we compute the binomial probability $P_{\geq i}(p_i)$ of getting i or more events with p values $\leq p_i$:

$$P_{\geq i}(p_i) = \sum_{k=i}^N \frac{N!}{(N-k)!k!} p_i^k (1-p_i)^{N-k}. \quad (3)$$

Here N is the number of HEN events analysed (158 in the 60-500 Hz band and 14 in the 500-2000 Hz band), and N_{tail} is the number of the smallest p values we wish to test. We choose N_{tail} to be 5% of N ; i.e., $N_{\text{tail}} = 8$ for the low frequency band and $N_{\text{tail}} = 1$ for the high frequency band.

The lowest $P_{\geq i}(p_i)$ for $i \in [1, N_{\text{tail}}]$ is taken as the most significant deviation from the null hypothesis. To assess the significance of the deviation, we repeat the test using p values drawn from a uniform distribution and count the fraction of such trials which give a lowest $P_{\geq i}(p_i)$ smaller

than that computed from the true measured p values.

Figures 5 and 6 show the cumulative distribution of p values measured in the low- and high-frequency analyses. In both cases the measured p values are consistent with the null hypothesis.

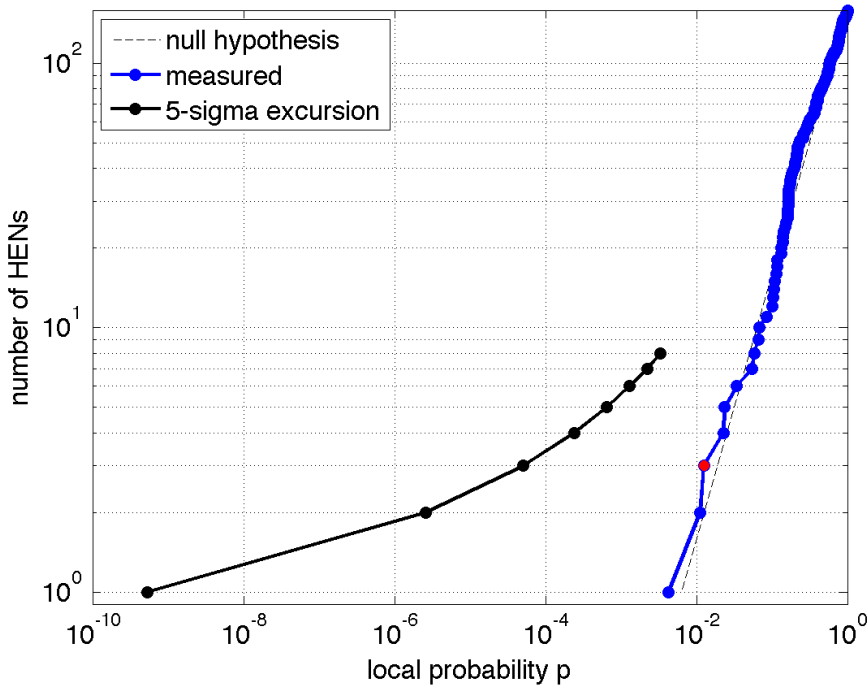


Fig. 5.— Distribution of observed p values for the loudest GW event associated with each neutrino analysed in the low frequency analysis. The red dot indicates the largest deviation of the low p tail from the uniform distribution null hypothesis; this occurs due to having the three loudest events below $p_3 \sim 0.013$. Deviations this large or larger occur in approximately 64% of experiments under the null hypothesis. The black line shows the threshold for a 5-sigma deviation from the null hypothesis.

5.3. GW upper limits

The sensitivity of the GW search is determined by a Monte-Carlo analysis. For each neutrino trigger, we add simulated GW signals to the on-source data and repeat the analysis described in Section 4.2. We consider a simulated signal detected if it produces an event louder than the loudest on-source event after all event tests have been applied. We define a 90% confidence level lower limit on the distance to the source as the maximum distance $D_{90\%}$ such that for any distance $D \leq D_{90\%}$ the probability of detection is 0.9 or greater.

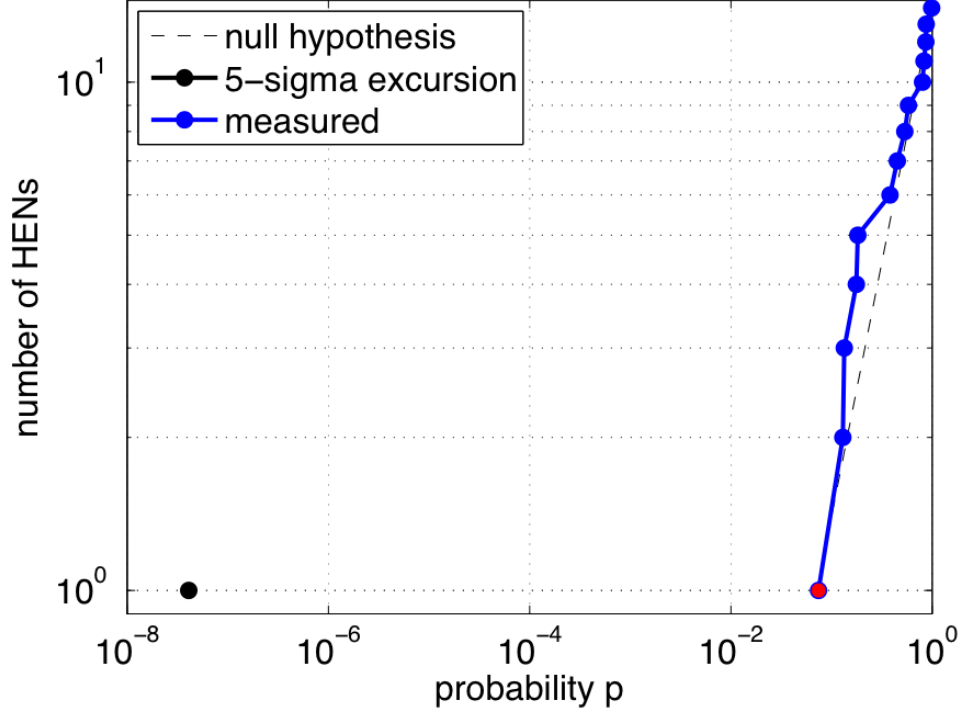


Fig. 6.— Distribution of observed p values for the loudest GW event associated with each neutrino analysed in the high frequency analysis. The red dot indicates the largest deviation of the low p tail from the uniform distribution null hypothesis; since $N_{\text{tail}} = 1$, this is constrained to occur for p_1 . Deviations this large or larger occur in approximately 66% of experiments under the null hypothesis. The black dot shows the threshold for a 5-sigma deviation from the null hypothesis.

5.3.1. Injected waveforms

As in GRB-triggered searches, we use a mix of *ad hoc* and astrophysically motivated GW waveforms. The *ad hoc* waveforms are Gaussian-modulated sinusoids:

$$h_+ = \frac{(1 + \cos^2 \iota)}{2} \frac{h_{\text{rss}}}{(2\pi\tau^2)^{\frac{1}{4}}} e^{-\frac{(t-t_0)^2}{4\tau^2}} \cos 2\pi f_0(t - t_0), \quad (4)$$

$$h_\times = \cos \iota \frac{h_{\text{rss}}}{(2\pi\tau^2)^{\frac{1}{4}}} e^{-\frac{(t-t_0)^2}{4\tau^2}} \sin 2\pi f_0(t - t_0). \quad (5)$$

Here f_0 is the central frequency, t_0 is the central time, and we chose $\tau = 1/f_0$ as the duration. We use central frequencies of 100 Hz, 150 Hz, and 300 Hz for the low-frequency analysis and 554 Hz and 1000 Hz for the high-frequency search. The quantity h_{rss} is the root-sum-square signal amplitude:

$$h_{\text{rss}} \equiv \sqrt{\int h_+^2(t) + h_\times^2(t) dt}. \quad (6)$$

This amplitude is related to the total energy E_{GW} in the gravitational-wave burst by:

$$E_{\text{GW}} = \frac{2}{5} \frac{\pi^2 c^3}{G} h_{\text{rss}}^2 f_0^2 D^2. \quad (7)$$

This waveform is consistent with the GW emission from a rotating system viewed from an inclination angle ι to the rotational axis. We select the inclination uniformly in $\cos \iota$ with $\iota \in [0^\circ, 5^\circ]$. This corresponds to a nearly on-axis system, such as would be expected for association with an observed long GRB.

For astrophysical injections we use the gravitational-wave emission of inspiraling neutron star and black hole binaries, which are widely thought to be the progenitors of short GRBs. Specifically, we use the post-Newtonian model for the inspiral of a double neutron star system with component masses $m_1 = m_2 = 1.35M_\odot$, and the one for a black-hole - neutron-star system with $m_1 = 5M_\odot$, $m_2 = 1.35M_\odot$. We set the component spins to zero in each case. Motivated by estimates of the jet opening angle for short GRBs, we select the inclination uniformly in $\cos \iota$ with $\iota \in [0^\circ, 30^\circ]$.

For each HEN trigger, the injections are distributed uniformly in time over the on-source window. The injection sky positions are selected randomly following the estimated probability distribution (2) for the HEN trigger, to account for the uncertainty in the true HEN direction of incidence. The polarization angle (orientation of the rotational axis on the sky) is distributed uniformly. Finally, the amplitude and arrival time at each detector is perturbed randomly to simulate the effect of calibration errors in the LIGO and VIRGO detectors.

5.3.2. Exclusion distances

For each waveform type (sine-Gaussians at 100, 150, 300, 554, 1000 Hz, and $1.35M_\odot - 1.35M_\odot$ and $5M_\odot - 1.35M_\odot$ inspirals) injections are performed over a range of amplitudes. For the inspiral signals, each amplitude corresponds to a well-defined distance. We can associate a physical distance to each amplitude for the sine-Gaussian waveforms as well, by assuming a fixed energy in gravitational waves. For concreteness, we select $E_{\text{GW}} = 10^{-2}M_\odot c^2$. This value corresponds to the optimistic limit of possible gravitational-wave emission by various processes in the collapsing cores of rapidly rotating massive stars (Fryer et al. 2002; Kobayashi & Mészáros 2003; Piro & Pfahl 2007; Fryer & New 2011), more conservative estimates based on 3D simulations have been made in (Dimmelmeier et al. 2008; Ott 2009; Scheidegger et al. 2010; Ott et al. 2011; Takiwaki & Kotake 2011). Our 90% confidence level lower limit on the distance to a GW source associated with a given HEN trigger is then the maximum distance $D_{90\%}$ such that for any distance $D \leq D_{90\%}$ there is a probability of at least 0.9 that such a GW signal would have produced an event louder than the loudest on-source event actually measured. For each type of gravitational wave simulated, the distributions of exclusion distances for our neutrino sample are shown in Figures 7 and 8. For binary neutron star systems of $(1.35 - 1.35)M_\odot$ and black hole - neutron star systems of $(5 - 1.35)M_\odot$ typical distance limits are 5 Mpc and 10 Mpc respectively. For the sine-Gaussian waveforms in the

low-frequency band the typical distance limits are between 5 Mpc and 17 Mpc, while for those in the high-frequency band the typical limits are of order 1 Mpc.

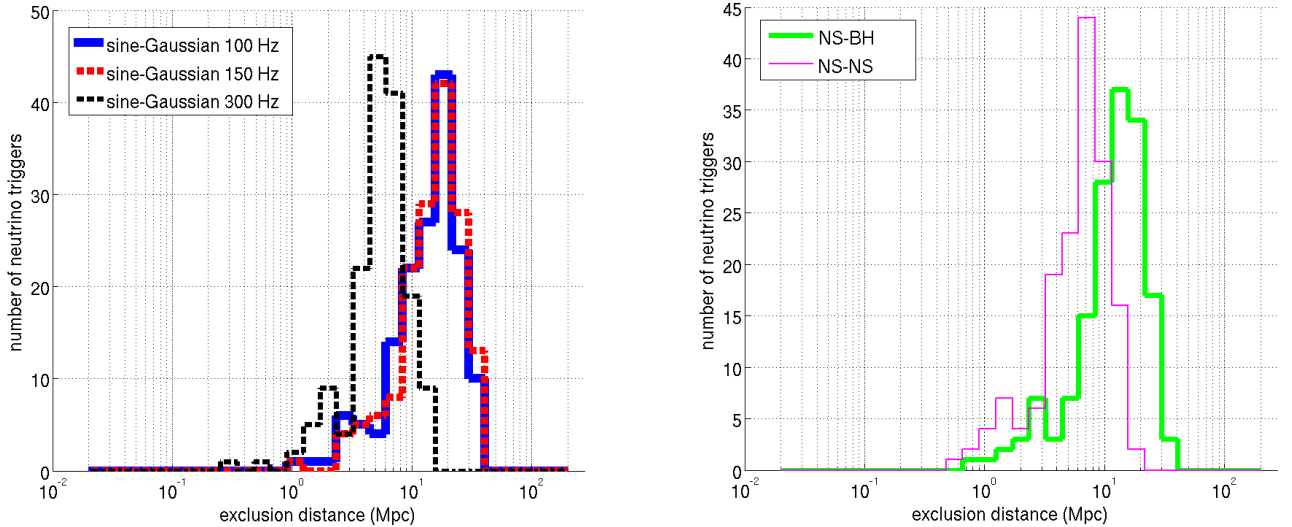


Fig. 7.— Low-frequency analysis: the top plot is the histogram for the sample of analysed neutrinos of the distance exclusions at the 90% confidence level for the 3 types of circular sine-Gaussian models considered: 100 Hz, 150 Hz and 300 Hz. A standard siren gravitational wave emission of $E_{GW} = 10^{-2} M_{\odot} c^2$ is assumed. The bottom plot shows histogram across the sample of analysed neutrinos of the distance exclusions at the 90% confidence level for the 2 families of binary inspiral models considered: NS-NS and BH-NS.

6. Astrophysical implications

Observational constraints on joint sources of GW and HEN signals have been derived in [Bartos et al. \(2011\)](#). However, they are based on the interpretation and the combination of previously published and independent GW and HEN observational results. The results presented in this section are the first derived from a joint GW-HEN analysis, using concomitant data obtained with LIGO/VIRGO and ANTARES.

6.1. Upper limits on GW-HEN populations

The present search for GW and HEN correlations in space and time revealed no evidence for coincident events. This implies a 90% confidence level upper limit on the rate of detectable coincidences of $2.3/T_{\text{obs}}$, where $T_{\text{obs}} \approx 100$ days is the duration of coincident observations. This can be expressed as a limit on the rate density (number per unit time per unit volume) $\rho_{\text{GW-HEN}}$

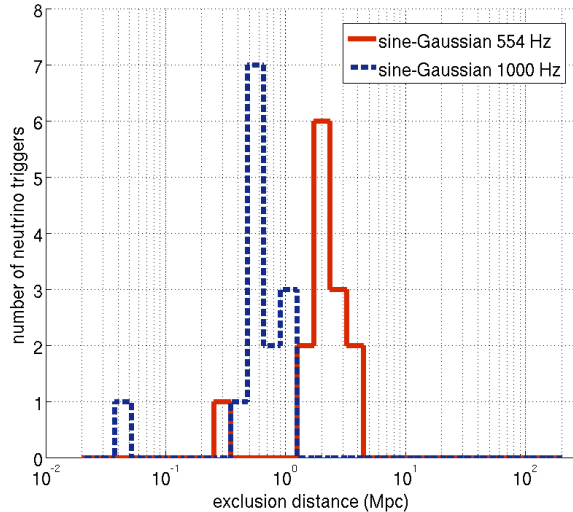


Fig. 8.— High-frequency analysis: the histogram for the sample of analysed neutrinos of the distance exclusions at the 90% confidence level for the 2 frequencies of circular sine-Gaussian models considered: 554 Hz and 1000 Hz.

of objects which would yield coincident GW and HEN signals as follows:

$$\rho_{\text{GW-HEN}} V_{\text{GW-HEN}} \leq \frac{2.3}{T_{\text{obs}}}. \quad (8)$$

In this expression, $V_{\text{GW-HEN}}$ is the volume of universe probed by the present analysis for typical GW-HEN sources. This volume is related to the GW and HEN detection efficiencies as a function of distance, and must be estimated for typical emission models.

We take as fiducial sources choked or failed GRBs, more generally two classes of objects: the final merger phase of the coalescence of two compact objects (short GRB-like), or the collapse of a massive object (long GRB-like), both followed by the emission of a relativistic hadronic jet. In the case of short GRBs (SGRB), the HEN horizon is estimated to be 4 Mpc using [Guetta et al. \(2004\)](#), while the typical GW horizon from the inspiral model is 5 - 10 Mpc depending on the binary masses. For long GRBs (LGRB) the HEN horizon increases to 12 Mpc using [Guetta et al. \(2004\)](#). The GW emission associated with long GRBs is highly uncertain; our optimistic assumption of $E_{\text{GW}} = 10^{-2} M_{\odot} c^2$ at low frequencies gives a typical horizon distance of 10-20 Mpc in GW. Using the lower of the GW and HEN distances in each case yields from equation (8) approximate limits on the population density of $\rho_{\text{GW-HEN}}^{\text{SGRB}} \lesssim 10^{-2} \text{Mpc}^{-3} \text{yr}^{-1}$ for SGRB-like sources, related to the merger of two compact objects, and $\rho_{\text{GW-HEN}}^{\text{LGRB}} \lesssim 10^{-3} \text{Mpc}^{-3} \text{yr}^{-1}$ for LGRB-like sources, related to the collapse of massive stars.

6.2. Comparison of limits with existing estimates

Nakar (2007); Guetta et al. (2004) suggest a local rate density of SGRB of $\rho_{\text{SGRB}} \lesssim 10^{-9} \text{Mpc}^{-3} \text{yr}^{-1}$, and the abundance of binary neutron star mergers, their assumed progenitors, is estimated to be $\rho_{\text{NS+NS}} \sim 10^{-6} \text{Mpc}^{-3} \text{yr}^{-1}$ (Kalogera et al. 2004; Belczynski et al. 2011), well below the reach of the present search ($\rho_{\text{GW-HEN}}^{\text{SGRB}} \lesssim 10^{-2} \text{Mpc}^{-3} \text{yr}^{-1}$). With $T_{\text{obs}} = 1 \text{ yr}$, an improvement of a factor 10 on the detection distance is required in order to be able to constrain the fraction of mergers producing coincident GW–HEN signals.

Guetta et al. (2004) estimate a total rate of long GRBs of $\rho_{\text{LGRB}} \sim 3 \times 10^{-8} \text{Mpc}^{-3} \text{yr}^{-1}$; these sources are closely related to Type II and Type Ibc core-collapse supernovae. The local rate of SNIbc is $\rho_{\text{SNIbc}} \sim 2 \times 10^{-5} \text{Mpc}^{-3} \text{yr}^{-1}$ (Guetta & Valle 2007), whereas $\rho_{\text{SNII}} \sim 2 \times 10^{-4} \text{Mpc}^{-3} \text{yr}^{-1}$ (Bazin et al. 2009), relatively close to the obtained limit $\rho_{\text{GW-HEN}}^{\text{LGRB}} \lesssim 10^{-3} \text{Mpc}^{-3} \text{yr}^{-1}$ under our optimistic assumptions of GW emission in this scenario. A factor 10 only is required in order to constrain the fraction of star collapses producing coincident GW–HEN signals, which translates into a required improvement of 2 on the detection distance.

7. Conclusions

This first joint GW–HEN search using 2007 data, obtained with the ANTARES HEN Telescope and the VIRGO/LIGO GW interferometers, opens the way to a novel and exciting multi-messenger astronomy. Promising limits on the rate density $\rho_{\text{GW-HEN}}$ of joint GW–HEN emitting systems were extracted for the first time using the analysis of coincident GW–HEN data. We note that these limits are consistent with the ones obtained in Bartos et al. (2011) derived from independent GW–HEN observations. More stringent limits will be available by performing similar coincidence analyses using other data sets provided by the same instruments.

For instance, the sixth LIGO science run S6 and second and third VIRGO science runs VSR2,3 covered the period from 7 July 2009 to 21 October 2010. Meanwhile, the ANTARES telescope has taken data with first 10 then 12 active lines since the end of December 2007. Their enhanced sensitivities should permit a combined analysis to gain the factor required to obtain $\rho_{\text{GW-HEN}}^{\text{LGRB}} \leq \rho_{\text{SNII/SNIbc}}$ and constrain for the first time the fraction of star collapses accompanied by the coincident emission of relativistic jets beamed towards Earth. The analysis of these data is underway.

Future schedules involving next-generation detectors with a sensitivity increased by at least one order of magnitude, such as KM3NET (Hernandez-Rey 2009) and the advanced LIGO/advanced VIRGO projects (Harry et al. 2010), are likely to coincide as well. They will give other opportunities to look for potential coincident GW–HEN emissions.

8. Acknowledgments

The authors gratefully acknowledge the support of the United States National Science Foundation for the construction and operation of the LIGO Laboratory, the Science and Technology Facilities Council of the United Kingdom, the Max-Planck-Society, and the State of Niedersachsen/Germany for support of the construction and operation of the GEO600 detector, and the Italian Istituto Nazionale di Fisica Nucleare and the French Centre National de la Recherche Scientifique for the construction and operation of the VIRGO detector. The authors also gratefully acknowledge the support of the research by these agencies and by the Australian Research Council, the International Science Linkages program of the Commonwealth of Australia, the Council of Scientific and Industrial Research of India, the Istituto Nazionale di Fisica Nucleare of Italy, the Spanish Ministerio de Educación y Ciencia, the Conselleria d’Economia Hisenda i Innovació of the Govern de les Illes Balears, the Foundation for Fundamental Research on Matter supported by the Netherlands Organisation for Scientific Research, the Polish Ministry of Science and Higher Education, the FOCUS Programme of Foundation for Polish Science, the Royal Society, the Scottish Funding Council, the Scottish Universities Physics Alliance, The National Aeronautics and Space Administration, the Carnegie Trust, the Leverhulme Trust, the David and Lucile Packard Foundation, the Research Corporation, and the Alfred P. Sloan Foundation.

The authors also acknowledge the financial support of the funding agencies for the construction and operation of the ANTARES neutrino telescope: Centre National de la Recherche Scientifique (CNRS), Commissariat à l’énergie atomique et aux énergies alternatives (CEA), Agence National de la Recherche (ANR), Commission Européenne (FEDER fund and Marie Curie Program), Région Alsace (contrat CPER), Région Provence-Alpes-Cote d’Azur, Département du Var and Ville de La Seyne-sur-Mer, France; Bundesministerium für Bildung und Forschung (BMBF), Germany; Istituto Nazionale di Fisica Nucleare (INFN), Italy; Stichting voor Fundamenteel Onderzoek der Materie (FOM), Nederlandse organisatie voor Wetenschappelijk Onderzoek (NWO), the Netherlands; Council of the President of the Russian Federation for young scientists and leading scientific schools supporting grants, Russia; National Authority for Scientific Research (ANCS), Romania; Ministerio de Ciencia e Innovacion (MICINN), Prometeo of Generalitat Valenciana (GVA) and Multi-Dark, Spain. They also acknowledge the technical support of Ifremer, AIM and Foselev Marine for the sea operation and the CC-IN2P3 for the computing facilities. This publication has been assigned LIGO Document Number LIGO-P1200006.

REFERENCES

- Abadie, J., et al. 2010, *Phys. Rev. D*, 81, 102001
- Abbott, B., et al. 2008a, *The Astrophysical Journal*, 683
- . 2008b, *Phys. Rev. D*, 77
- . 2009, *Rep. Prog. Phys.*, 72, 076901

- . 2010, *The Astrophysical Journal*, 715, 1438
- Accadia, T., et al. 2012, *Journal of Instrumentation*, 7, P03012
- Acernese, F., et al. 2008, *Class. Quantum Gravity*, 25, 114045
- Ageron, M., et al. 2011, *Nucl. Instr. and Meth., A* 656, 11
- Aguilar, J. A., et al. 2011, *Astroparticle Physics*, 34, 652
- Ando, S., et al. 2012, submitted to *Rev. Mod. Phys.*, eprint 1203.5192
- Aso, Y., et al. 2008, *Class. Quantum Grav.*, 25, 114039
- Bahcall, J., & Waxman, E. 1997, *Phys. Rev. Lett.*, 78, 2292
- Baret, B., et al. 2011, *Astroparticle Physics*, 35, 1
- Bartos, I., et al. 2011, *Phys. Rev. Lett.*, 107, 251101
- Bazin, G., et al. 2009, *Astronomy & Astrophysics*, 499, 653
- Belczynski, K., et al. 2011, *Proceedings of The Rencontres de Moriond and GPhyS colloquium, La Thuile, Italy*, eprint 1106.0397
- Berezinsky, V., et al. 2011, *Phys. Rev. D*, 84, 085006
- Braccini, S., et al. 2005, *Astroparticle Physics*, 23, 557
- Brady, P. R., Wiseman, A. G., & Creighton, J. D. E. 2004, *Class. Quantum Grav.*, 21, S1775
- Bromberg, O., et al. 2012, *The Astrophysical Journal*, 749
- Campana, S., et al. 2006, *Nature*, 442, 1008
- Corsi, A., & Mészáros, P. 2009, *The Astrophysical Journal*, 702, 1171
- Corsi, A., & Owen, B. J. 2011, *Phys. Rev. D*, 83, 104014
- Damour, T., & Vilenkin, A. 2000, *Phys. Rev. Lett.*, 85, 3761
- Davies, M. B., et al. 2002, *The Astrophysical Journal*, 579, L63
- de Freitas Pacheco, J. A. 1998, *Astronomy & Astrophysics*, 336, 397
- Dimmelmeier, H., et al. 2008, *Phys. Rev. D*, 78
- Duncan, R. C., & Thompson, C. 1992, *Astrophysical Journal Letters*, 392, L9
- Eichler, D., et al. 1989, *Nature*, 340, 126

- Fryer, C., & New, K. 2011, *Living Rev. Relativity*, 14
- Fryer, C., et al. 2002, *The Astrophysical Journal*, 565, 430
- Galama, T. J., et al. 1998, *Nature*, 395, 670
- Gehrels, N., et al. 2006, *Nature*, 444, 1044
- Guetta, D., & Valle, M. D. 2007, *Astroparticle Physics*, 657, L73
- Guetta, D., et al. 2004, *Astroparticle Physics*, 20, 429
- Halladjian, G. 2010, PhD thesis, Université de la Méditerranée- Aix Marseille II, Marseille, France,
<http://antares.in2p3.fr/index.html>
- Harry, G. M., et al. 2010, *Classical and Quantum Gravity*, 27, 084006
- Hernandez-Rey, J. J. 2009, *J. Phys. Conf. Ser.*, 171, 012047
- Hjorth, J., et al. 2003, *Nature*, 413, 6942
- Ioka, K. 2001, *Mon. Not. Roy. Astron. Soc.*, 327, 639
- Kalogera, V., et al. 2004, *ApJ*, 601, L179
- Kobayashi, S., & Mészáros, P. 2003, *The Astrophysical Journal*, 589, 861
- Kotake, K., et al. 2006, *Rep. Prog. Phys.*, 69, 971
- Kouveliotou, C., et al. 1993, *Astrophysical Journal Letters*, 413, L101
- M. Shibata, S. K., & Eriguchi, Y. 2003, *Mon. Not. Roy. Astron. Soc.*, 343
- MacFadyen, A. I., & Woosley, S. E. 1999, *The Astrophysical Journal*, 524, 262
- Malesani, D., et al. 2004, *The Astrophysical Journal*, 609, L5
- Meszáros, P. 1999, *Astron. Astrophys. Suppl. Ser.*, 138, 533
- Meszáros, P., & Waxman, E. 2001, *Phys. Rev. Lett.*, 87, 171102
- Mosquera Cuesta, H. J., & González, D. M. 2001, *Phys. Lett. B*, 500, 215
- Nakar, E. 2007, *Phys. Rept.*, 442, 166
- Ott, C., et al. 2011, *Phys. Rev. Lett*, 106
- Ott, C. D. 2009, *Classical and Quantum Gravity*, 26, 063001
- Piro, A. L., & Pfahl, E. 2007, *The Astrophysical Journal*, 658, 1173

- Pradier, T. 2009, *Nucl. Instr. and Meth., A* 602, 268
- R. Narayan, B. P., & Piran, T. 1992, *Astrophysical Journal Letters*, 395, L83
- Scheidegger, S., et al. 2010, *Astronomy and Astrophysics*, 514
- Siemens, X., et al. 2006, *Phys. Rev. D*, 73, 105001
- Stanek, K. Z., et al. 2003, *The Astrophysical Journal*, 591, L17
- Sutton, P. J., et al. 2010, *New J. Phys*, 12, 053034
- Takiwaki, T., & Kotake, K. 2011, *The Astrophysical Journal*, 743
- Thompson, C., & Duncan, R. C. 1995, *Mon. Not. Roy. Astron. Soc.*, 275, 255
- van Hoven, M., & Levin, Y. 2011, *The Royal Astronomical Society*, 410, 1036
- Was, M., et al. 2012, submitted to *Phys. Rev. D*, eprint 1201.5599
- Waxman, E. 2001, *Lect. Notes Phys.*, 576, 122
- Woosley, S. E., & Bloom, J. S. 2006, *Annual Review of Astronomy & Astrophysics*, 44, 507
- Zink, B., Kokkotas, K. D., & Lasky, P. D. 2012, *Phys. Rev. D*, 85, 024030